

---

SI<sup>3</sup>

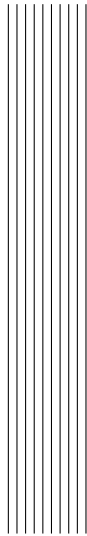
Sea Ice modelling Integrated Initiative  
The NEMO Sea Ice engine

---

Martin Vancoppenolle, Clément Rousset, Ed Blockley, and the Sea Ice Working Group

ISSN No 1288-1619

January 13, 2023



# Contents

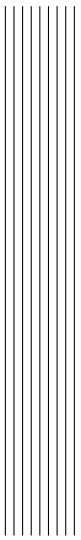
<b>1</b>	<b>Model Basics</b>	<b>5</b>
1.1	Rationale and assumptions . . . . .	6
1.1.1	Scales, thermodynamics and dynamics . . . . .	6
1.1.2	Subgrid scale variations . . . . .	6
1.1.3	Thermodynamic formulation . . . . .	7
1.1.4	Dynamic formulation . . . . .	9
1.2	Thickness distribution framework . . . . .	9
1.3	Governing equations . . . . .	11
1.4	Ice Dynamics . . . . .	12
1.5	Ice thermodynamics . . . . .	13
1.5.1	Transport in thickness space . . . . .	14
1.5.2	Thermodynamic source and sink terms . . . . .	14
<b>2</b>	<b>Time, space and thickness space domain</b>	<b>19</b>
2.1	Time domain . . . . .	19
2.2	Spatial domain . . . . .	20
2.3	Thickness space domain . . . . .	21
<b>3</b>	<b>Ice dynamics</b>	<b>25</b>
3.1	Representation of sea ice drift in $SI^3$ . . . . .	26
3.1.1	Basal stress and landfast sea ice . . . . .	27
3.1.2	Ice strength and tensile strength . . . . .	27
3.1.3	Namelist parameters . . . . .	27
3.2	The interaction force, deformation, internal stresses . . . . .	27

---

3.3	The viscous-plastic (VP) line-successive relaxation (LSR) solver . . . . .	30
3.3.1	The VP rheology . . . . .	30
3.3.2	The LSR numerical approach . . . . .	30
3.4	EVP solvers . . . . .	32
3.5	The EAP solver . . . . .	32
3.5.1	The EAP rheology . . . . .	32
3.5.2	The EAP solver . . . . .	32
<b>4</b>	<b>Ice transport</b> . . . . .	<b>33</b>
4.1	Second order moments conserving (Prather 1986) scheme ( <i>ln_adv_Pra</i> ) . . . . .	34
4.2	5 <sup>th</sup> order flux-corrected transport scheme (UM5) . . . . .	34
<b>5</b>	<b>Ridging and rafting</b> . . . . .	<b>35</b>
5.1	Theory . . . . .	37
5.1.1	Dynamical inputs . . . . .	37
5.1.2	The two deformation modes: ridging and rafting . . . . .	38
5.1.3	Participation functions . . . . .	38
5.1.4	Transfer functions . . . . .	39
5.1.5	Ridging shift . . . . .	40
5.1.6	Mechanical redistribution for other global ice variables . . . . .	41
<b>6</b>	<b>Ice thermodynamics</b> . . . . .	<b>43</b>
6.1	Overarching aspects and practical features . . . . .	44
6.1.1	From / to temperature and enthalpy . . . . .	46
6.1.2	Control corrections . . . . .	46
6.2	Approximate energy budget of the first-ocean level . . . . .	46
6.3	Lateral thermodynamics . . . . .	47
6.3.1	Ice growth in open water . . . . .	47
6.3.2	Lateral melting . . . . .	48
6.4	Vertical thermodynamics . . . . .	50
6.4.1	Thermal diffusion (temperature calculation) . . . . .	50
6.4.2	Radiation attenuation and absorption . . . . .	52
6.4.3	Vertical accretion and ablation . . . . .	52
6.4.4	Remapping . . . . .	54
6.5	Transport in thickness space . . . . .	55
6.6	Melt ponds . . . . .	57
6.7	Ice salinity . . . . .	58
6.8	Single-category use . . . . .	59
6.9	Ice age . . . . .	60
<b>7</b>	<b>Radiative transfer</b> . . . . .	<b>63</b>
7.1	Solar radiation partitioning in the snow-ice system . . . . .	65
7.1.1	Surface albedo . . . . .	66
7.1.2	Transmission below the snow/ice surface . . . . .	69

---

7.1.3	Attenuation and transmission below the ice/ocean interface	69
7.2	Solar radiation: framing sea ice at the ocean-atmosphere boundary	69
7.2.1	Forced mode	70
7.2.2	Coupled mode	70
<b>8</b>	<b>Output and diagnostics</b>	<b>73</b>
8.1	SIMIP diagnostics	74
8.1.1	Missing SIMIP fields	74
8.1.2	Links	75
8.2	Conservation checks	75
<b>9</b>	<b>Guidelines for documenting the code</b>	<b>77</b>
9.1	Overarching aspects and practical features	77
9.2	Calculation step 1	78
9.3	Calculation step 2	78
	<b>Bibliography</b>	<b>79</b>
	<b>Index</b>	<b>85</b>



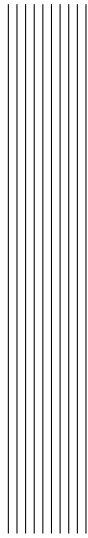
## Disclaimer

Like all components of NEMO, the sea ice component is developed under the **CE-CILL license**, which is a French adaptation of the GNU GPL (General Public License). Anyone may use it freely for research purposes, and is encouraged to communicate back to the NEMO team its own developments and improvements. The model and the present document have been made available as a service to the community. We cannot certify that the code and its manual are free of errors. Bugs are inevitable and some have undoubtedly survived the testing phase. Users are encouraged to bring them to our attention. The authors assume no responsibility for problems, errors, or incorrect usage of NEMO.

SI3 reference in papers and other publications is as follows:

Vancoppenolle, M., Rousset, C., Blockley, E., and the NEMO Sea Ice Working Group, 2023: SI<sup>3</sup> – Sea Ice modelling Integrated Initiative – The NEMO Sea Ice Engine, doi:10.5281/zenodo.7534900, 2023.

Additional information can be found on [www.nemo-ocean.eu](http://www.nemo-ocean.eu).



# Introduction

## Abstract

SI<sup>3</sup> (Sea Ice modelling Integrated Initiative) is the sea ice engine of NEMO (Nucleus for European Modelling of the Ocean). It is adapted to regional and global sea ice and climate problems. It is intended to be a flexible tool for studying sea ice and its interactions with the other components of the Earth System over a wide range of space and time scales. For these applications, a 2+1D continuum approach is currently the most appropriate (Blockley et al., 2020), SI<sup>3</sup> is based on the Arctic Ice Dynamics Joint EXperiment (AIDJEX) framework (Coon et al., 1974), combining the ice thickness distribution framework, the conservation of horizontal momentum, an elastic-viscous plastic rheology, and energy-conserving halothermodynamics. Prognostic variables are the two-dimensional horizontal velocity field, ice volume, area, enthalpy, salt content, snow volume and enthalpy, and melt pond volume and area. In the horizontal direction, the model uses a curvilinear orthogonal grid. In the vertical direction, the model uses equally-spaced layers. In thickness space, the model uses thickness categories with prescribed boundaries. Various physical and numerical choices are available to describe sea ice physics. SI<sup>3</sup> is interfaced with the NEMO ocean engine, and, via the OASIS coupler, with several atmospheric general circulation models. It also supports two-way grid embedding via the AGRIF software.

## Approach and history

The sea Ice Modelling Integrated Initiative (SI<sup>3</sup>) is the sea ice engine of the Nucleus for European Modelling of the Ocean (NEMO). It is intended to be a flexible tool for studying sea ice and its interactions with the other components of the Earth System over a wide range of space and time scales. SI<sup>3</sup> is a curvilinear grid, finite-difference implementation of the classical AIDJEX<sup>1</sup> model (Coon et al., 1974), combining the conservation of momentum for viscous-plastic continuum, energy and salt-conserving halo-thermodynamics (Bitz and Lipscomb, 1999; Vancoppenolle et al., 2009a), an explicit representation of subgrid-scale ice thickness variations, snow and melt ponds (Flocco and Feltham, 2007). An option to switch back to the *single-category* (or *2-level*) framework of Hibler (1979) provides a reasonably cheap sea ice modelling solution.

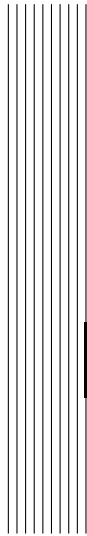
SI<sup>3</sup> is the result of the recommendation of the Sea Ice Working Group (SIWG) to reduce duplication and better use development resources. SI<sup>3</sup> merges the capabilities of the 3 formerly used NEMO sea ice models (CICE, GELATO and LIM). The **3** in SI<sup>3</sup> refers to the three formerly used sea ice models. It also refers to linkages between 3 different media (ocean, ice, snow). The model can be spelt 'SI3' in situations where the superscript could be problematic (i.e., within code and svn repository etc.) The model name would be pronounced as 'si-cube' for short (or 'sea ice cubed' for slightly longer).

Some of SI<sup>3</sup>'s underlying assumptions are:

- Sea ice is frozen seawater, in tight interaction with the underlying ocean. This close connexion suggests that the sea ice and ocean model components must be as consistent as possible. In practice, this is materialized by the close match between LIM and NEMO, in terms of numerical choices, regarding the grid (Arakawa C-type) and the numerical discretization (finite differences with NEMO scale factors).
- It is useful to be able to either prescribe the atmospheric state or to use an atmospheric model. For consistency and simplicity of the code, we choose to use formulations as close as possible in both cases.
- Different resolutions and time steps can be used. There are parameters that depend on such choices. We thried to achieve a resolution and time-step independent code, by imposing a priori scaling on the resolution / time step dependence of such parameters.
- Energy, mass and salt must be conserved as much as possible.

---

<sup>1</sup>AIDJEX=Arctic Ice Dynamics Joint EXperiment



# 1 Model Basics

## Contents

---

<b>1.1 Rationale and assumptions</b> . . . . .	<b>6</b>
1.1.1 Scales, thermodynamics and dynamics . . . . .	6
1.1.2 Subgrid scale variations . . . . .	6
1.1.3 Thermodynamic formulation . . . . .	7
1.1.4 Dynamic formulation . . . . .	9
<b>1.2 Thickness distribution framework</b> . . . . .	<b>9</b>
<b>1.3 Governing equations</b> . . . . .	<b>11</b>
<b>1.4 Ice Dynamics</b> . . . . .	<b>12</b>
<b>1.5 Ice thermodynamics</b> . . . . .	<b>13</b>
1.5.1 Transport in thickness space . . . . .	14
1.5.2 Thermodynamic source and sink terms . . . . .	14

---

## 1.1 Rationale and assumptions

- Drift and deformation are horizontal, heat transfer is vertical;
- Dynamics: sea ice is a non-newtonian 2D continuum;
- Thermodynamics: sea ice is a mushy layer covered by snow;
- Ice properties, in particular thickness, are not uniform at the grid cell scale for current model applications.

### 1.1.1 Scales, thermodynamics and dynamics

Because sea ice is much wider –  $\mathcal{O}(100\text{-}1000\text{ km})$  – than thick –  $\mathcal{O}(1\text{ m})$  – ice drift can be considered as purely horizontal: vertical motions around the hydrostatic equilibrium position are negligible. The same scaling argument justifies the assumption that heat exchanges are purely vertical<sup>1</sup>. It is on this basis that thermodynamics and dynamics are separated and rely upon different frameworks and sets of hypotheses: thermodynamics use the ice thickness distribution (Thorndike et al., 1975) and the mushy-layer (Worster, 1992) frameworks, whereas dynamics assume continuum mechanics (e.g., Leppäranta, 2005). Thermodynamics and dynamics interact by two means: first, advection impacts state variables; second, the horizontal momentum equation depends, among other things, on the ice state.

### 1.1.2 Subgrid scale variations

Sea ice properties – in particular ice thickness – feature important changes at horizontal scales  $\mathcal{O}(1\text{ m})$  (Thorndike et al., 1975). An explicit representation of these variations is not and will not be – at least in the next twenty years or so – accessible to large-scale sea ice models. Yet important features, such as energy exchanges through the ice, quite non-linearly depend on ice thickness (Maykut, 1986); whereas ice motion depends on the presence of open water, thin and thick ice at the very least, suggesting that subgrid-scale variations in ice properties must be accounted for, at least in a statistical fashion (Maykut and Thorndike, 1973).

The *multi-category* framework (Maykut and Thorndike, 1973) addresses this issue by treating the ice thickness as an independent variable next to spatial coordinates and time, and introducing a thickness distribution<sup>2</sup>  $g(h)$  as the main prognostic model field. In the discrete world, the thickness distribution is converted

<sup>1</sup>The latter assumption is probably less valid, because the horizontal scales of temperature variations are  $\mathcal{O}(10\text{-}100\text{ m})$

<sup>2</sup> $g(h)$ , termed the *ice thickness distribution* is the density of probability of ice thickness (Thorndike et al., 1975).

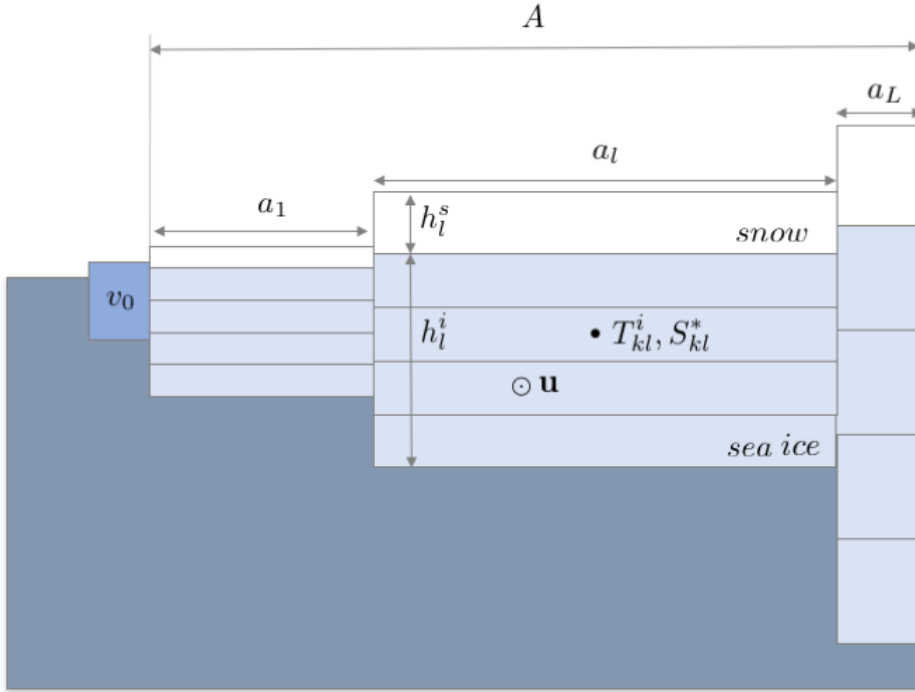


**Figure 1.1:** Representation of the ice pack, using multiple categories with specific ice concentration ( $a_l, l = 1, 2, \dots, L$ ), thickness ( $h_l^i$ ), snow depth ( $h_l^s$ ), vertical temperature and salinity profiles ( $T_{kl}^i, S_{kl}^*$ ) and a single ice velocity vector ( $\mathbf{u}$ ).

into  $jp1$  thickness categories. Ice thickness categories occupy a fraction of each grid cell, termed ice concentration ( $a_l, l = 1, 2, \dots, L$ ), with specific thickness and properties.

The *single-category* framework (Hibler, 1979) tackles the subgrid-scale issue by drastically simplifying the ice thickness distribution. The grid cell is divided into open water and sea ice characterized by a single ice concentration  $A$  and mean thickness  $H$ . Single-category models (in particular SI<sup>3</sup>2) typically add parameterizations to represent the effects of unresolved ice thickness distribution on ice growth and melt (see, e.g. Mellor and Kantha, 1989; Fichefet and Morales Maqueda, 1997).

SI<sup>3</sup> provides the choice between either a multi- or a single-category framework. The default mode is multi-category. The single-category mode can be activated by setting the number of categories ( $jp1=1$ ) and by activating the virtual thickness distribution parameterizations (`ln_virtual_itd`).

**Table 1.1:** Thermodynamic constants of the model.

	Description	Value	Units	Ref
$c_i$ (cpic)	Pure ice specific heat	2096.7	J/kg/K	Feistel and Wagner (2006)
$c_w$ (rcp)	Seawater specific heat	3991	J/kg/K	IOC, SCOR and IAPSO (2010)
$L$ (rLfus)	Latent heat of fusion (0°C)	$3.33360 \times 10^5$	J/kg/K	Feistel and Wagner (2006)
$L$ (rLsub)	Latent heat of sublimation (0°C)	$2.8344 \times 10^6$	J/kg/K	Feistel and Wagner (2006)
$\rho_i$ (rhoi)	Sea ice density	917	kg/m <sup>3</sup>	Pounder (1965)
$\rho_s$ (rhos)	Snow density	330	kg/m <sup>3</sup>	Maykut and Untersteiner (1971)
$\mu$ (rTmlt)	Linear liquidus coefficient	0.054	°C/(g/kg)	Assur (1958)

### 1.1.3 Thermodynamic formulation

Ice thermodynamics are formulated assuming that sea ice is covered by snow. Within each thickness category, both snow and sea ice are horizontally uniform, hence each thickness category has a specific ice thickness ( $h_i^l$ ) and snow depth ( $h_s^l$ ). Snow is assumed to be fresh, with constant density and thermal conductivity. Sea ice is assumed to be a *mushy layer*<sup>3</sup> (Worster, 1992) of constant density, made of pure ice and brine in thermal equilibrium, related by a linear liquidus relationship (Bitz and Lipscomb, 1999). A vertically-averaged bulk salinity  $S_l$  uniquely characterizes brine fraction for each thickness category, and changes through time from a simple parametrization of brine drainage. The linear vertical salinity profile ( $S_{kl}^*$ ) is reconstructed from the vertical mean (Vancoppenolle et al., 2009b). The diffusion of heat affects the vertical temperature profile, discretized on a unique layer of snow and multiple ice layers (typically 2-5) for each category, whereas thermal properties depend on local brine fraction. Growth and melt rates are computed, also for each ice category. The choice of the main thermodynamic constants is described in Tab. 1.1.

**Table 1.2:** SI<sup>3</sup> global variables.

Symbol	Description	Units	Code name
$\mathbf{u}$	Sea ice velocity	[m.s <sup>-1</sup> ]	<i>u_ice, v_ice (ji,jj)</i>
$\sigma$	Stress tensor	[Pa.m]	<i>stress1_i, stress2_i</i> <i>stress12_i (ji,jj)</i>
$a_l$	Concentration of sea ice in category $l$	[-]	<i>a_i(ji,jj,jl)</i>
$v_l^i$	Volume of sea ice per unit area in category $l$	[m]	<i>v_i(ji,jj,jl)</i>
$v_l^s$	Volume of snow per unit area in category $l$	[m]	<i>v_s(ji,jj,jl)</i>
$e_{kl}^i$	Sea ice enthalpy per unit area in layer $k$ and category $l$	[J.m <sup>-2</sup> ]	<i>e_i(ji,jj,jk,jl)</i>
$e_l^s$	Snow enthalpy per unit area in category $l$	[J.m <sup>-2</sup> ]	<i>e_s(ji,jj,jl)</i>
$M_l^s$	Sea ice salt content in category $l$	[g/kg.m]	<i>smv_i(ji,jj,jl)</i>

Temperature, salinity, ice thickness, and snow depth are not extensive variables

<sup>3</sup>Mushy layers are two-phase, two-component porous media.

and therefore not conservative. Hence, conservative, extensive variables, must be introduced to ensure mass, salt and energy conservation. There are several back-and-forth conversions from extensive (conservative) state variables (see Table 1.2) to intensive state variables of practical use (Table 1.3).

**Table 1.3:** Intensive variables of practical use.

Symbol	Description	Units
$h_l^i = v_l^i/g_l^i$	Ice thickness	[m]
$h_l^s = v_l^s/g_l^s$	Snow depth	[m]
$q_{m,kl}^i = e_{i,k}^i/(h_l^i/N)$	Ice specific enthalpy	[J.kg <sup>-1</sup> ]
$q_{m,l}^s = e_l^s/h_l^s$	Snow specific enthalpy	[J.kg <sup>-1</sup> ]
$T_{kl}^i = T(q_{kl}^i)$	Ice temperature	[K]
$T_l^s = T(q_l^s)$	Snow temperature	[K]
$\bar{S}_l^i = M_l^s/v_l^i$	Vertically-averaged bulk ice salinity	[g/kg]
$S_{kl}^*$	Depth-dependent ice salinity	[g/kg]
$\phi_{kl}$	Brine fraction	[-]

### 1.1.4 Dynamic formulation

The formulation of ice dynamics is based on continuum mechanics. The latter holds provided the drift ice particles are much larger than single ice floes, and much smaller than typical gradient scales (Feltham, 2008). This compromise is rarely achieved in practice (Leppäranta, 2005). Yet the continuum approach generates a convenient momentum equation for the horizontal ice velocity vector  $\mathbf{u} = (u, v)$ , which can be solved with classical numerical methods (here, finite differences on the NEMO C-grid). The dominant and most challenging term in the momentum equation is internal stress. We follow the continuum framework (Hibler, 1979), and assume by default a viscous-plastic (VP) rheology, by default assuming that sea ice has no tensile strength but responds to compressive and shear deformations in a plastic way. In practice, the elastic-viscous-plastic (aEVP) technique of (Bouillon et al., 2013) is used by default, more convenient numerically than VP.

## 1.2 Thickness distribution framework

We first present the essentials of the thickness distribution framework (Thorndike et al., 1975). Consider a given region of area  $R$  centered at spatial coordinates  $(\mathbf{x})$  at a given time  $t$ .  $R$  could be e.g. a model grid cell. The ice thickness distribution  $g(\mathbf{x}, t, h)$  is introduced as follows:

$$g(h) = \lim_{dh \rightarrow 0} \frac{dA(h, h + dh)}{dh}, \quad (1.1)$$

where  $dA(h, h + dh)$  is the surface fraction of all parts of  $R$  with ice thickness between  $h$  and  $h + dh$ . Using this definition, the spatial structure of ice thickness

is lost (see Fig. 1.2), and  $h$  becomes an extra independent variable, next to spatial coordinates and time, that can be thought as random.  $g$  is by definition normalized to 1. The conservation of area, expressed in terms of  $g(h)$ , is given by (Thorndike et al., 1975):

$$\frac{\partial g}{\partial t} = -\nabla \cdot (g\mathbf{u}) - \frac{\partial}{\partial h}(fg) + \psi, \quad (1.2)$$

where the terms on the right hand side refer to horizontal transport, thermodynamic transport in thickness space ( $f$ , m/s is the growth/melt rate), and mechanical redistribution rate, e.g. by ridging and rafting, where  $\psi$  must conserve ice area and volume by construction.

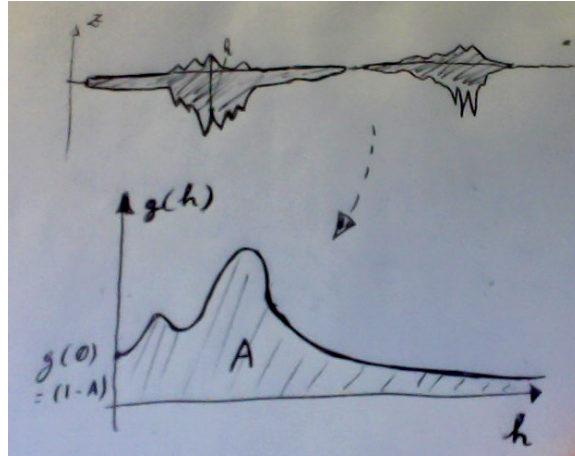


**Figure 1.2:** Representation of the relation between real thickness profiles and the ice thickness distribution function  $g(h)$

In numerical implementations, the thickness distribution is discretized into several thickness categories, with specific ice concentration  $a_l$  and ice volume per area  $v_l^i$ :

$$a_l = \int_{H_{l-1}^*}^{H_l^*} dh \cdot g(h), \quad (1.3)$$

$$v_l^i = \int_{H_{l-1}^*}^{H_l^*} dh \cdot h \cdot g(h). \quad (1.4)$$

Ice volume per area is the extensive counterpart for ice thickness, connected with volume through  $h_l^i = v_l^i/a_l$ . Evolution equations for extensive variables can be readily derived from equation 1.5 by integration between thickness boundaries of the  $l^{\text{th}}$  category (Bitz et al., 2001). This applies to all model extensive variables

(see Table 1.2). For ice area, this reads:

$$\frac{\partial a_l}{\partial t} = -\nabla \cdot (a_l \mathbf{u}) + \Theta_l^a + \int_{H_{l-1}^*}^{H_l^*} dh \psi. \quad (1.5)$$

where  $\Theta_l^a$  refers to the effect of thermodynamics. Enthalpy is a particular case because it also has a vertical depth dependence  $z$ , which corresponds to  $K$  vertical layers of equal thickness. The solution adopted here, following from Zhang and Rothrock (2001), is that enthalpy from the individual layers are conserved separately. This is a practical solution, for lack of better.

SI<sup>3</sup> resolves conservation equations for all extensive variables that characterize the ice state. Let us now connect this detailed information with classical sea ice fields. The ice concentration  $A$  and the ice volume per area<sup>4</sup>  $V_i$  (m) directly derive from  $g$ :

$$A(\mathbf{x}, t) = \int_{0^+}^{\infty} dh \cdot g(h, \mathbf{x}, t) \sim A_{ij} = \sum_{l=1}^L a_{ijl}, \quad (1.6)$$

$$V_i(\mathbf{x}, t) = \int_0^{\infty} dh \cdot g(h, \mathbf{x}, t) \cdot h \sim V_{ij}^i = \sum_{l=1}^L v_{ijl}^i. \quad (1.7)$$

$$(1.8)$$

where the  $0^+$  boundary implies that the means exclude open water. The mean ice thicknesses  $H_i$  (m) is:

$$H_i = V_i/A, \quad (1.9)$$

whereas the open water fraction is simply  $1 - A$ .

### 1.3 Governing equations

Let us now readily present the set of the SI<sup>3</sup> governing equations in the framework of the assumptions developed above. The conservation of horizontal momentum reads:

$$m \frac{\partial \mathbf{u}}{\partial t} = \nabla \cdot \boldsymbol{\sigma} + A(\boldsymbol{\tau}_a + \boldsymbol{\tau}_w) - m f \mathbf{k} \times \mathbf{u} - m g \nabla \eta, \quad (1.10)$$

where  $m = \rho_i V_i + \rho_s V_s$  is the ice and snow mass per unit area,  $\mathbf{u}$  is the ice velocity,  $\boldsymbol{\sigma}$  is the internal stress tensor,  $\boldsymbol{\tau}_a$  and  $\boldsymbol{\tau}_w$  are the air and ocean stresses, respectively,  $f$  is the Coriolis parameter,  $\mathbf{k}$  is a unit vector pointing upwards,  $g$  is the gravity acceleration and  $\eta$  is the ocean surface elevation. The continuum approach used

<sup>4</sup>Ice volume per area is equivalent to the grid-cell averaged ice thickness.

in SI<sup>3</sup> Bouillon et al. (2013) gives the stress tensor as a function of the strain rate tensor  $\dot{\epsilon}$  and some of the sea ice state variables:

$$\boldsymbol{\sigma} = \boldsymbol{\sigma}(\dot{\epsilon}, \text{ice state}). \quad (1.11)$$

To the exception of velocity and internal stress, all extensive variables in Table 1.2 follow a conservation equation of the form:

$$\frac{\partial X}{\partial t} = -\nabla \cdot (\mathbf{u}X) + \Theta^X + \Psi^X, \quad (1.12)$$

including the effects of transport, thermodynamics ( $\Theta^X$ ) and mechanical redistribution ( $\Psi^X$ ). Solving these  $jpl.(4 + 2.jpk)$  equations gives the temporal evolution of  $\mathbf{u}$ ,  $\boldsymbol{\sigma}$  and the rest of the global (extensive) variables listed in Table 1.2.

## 1.4 Ice Dynamics

Dynamical processes include the conservation of momentum, rheology, transport and mechanical redistribution. To resolve the momentum equation, atmospheric stress is taken either as forcing or from an atmospheric model, oceanic stress and sea surface elevation from the ocean model, the Coriolis term is trivial. The last term, the divergence of the internal stress tensor  $\boldsymbol{\sigma}$ , is the most critical term in the momentum equation and requires a rheological formulation. The continuum approach used in SI<sup>3</sup> gives the stress tensor components as (Bouillon et al., 2013):

$$\sigma_{ij} = \frac{P}{2(\Delta + \Delta_{min})} \left[ (\dot{\epsilon}_{kk} - \Delta)\delta_{ij} + \frac{1}{e^2}(2\dot{\epsilon}_{ij} - \dot{\epsilon}_{kk}\delta_{ij}) \right], \quad (1.13)$$

where  $\Delta$  is a particular measure of the deformation rate,  $\Delta_{min}$  a parameter determining a smooth transition from pure viscous flow ( $\Delta \ll \Delta_{min}$ ) to pure plastic flow ( $\Delta \gg \Delta_{min}$ ), and  $e$  is a parameter giving the ratio between the maximum compressive stress and twice the maximum shear stress. In the pure plastic regime, the stress principal components should lie on the edge of an elliptical yield curve (Fig. 6.2). In the viscous regime, they are within the ellipse. The ice strength  $P$  determines the plastic failure criterion and connects the momentum equation with the state of the sea ice.  $P$  is not well constrained and must be parameterized. The heuristic option of Hibler (1979) was here adopted as a reference formulation:

$$P = P^* V_i e^{-C(1-A)}, \quad (1.14)$$

where  $P^*$  and  $C$  are empirical constants (see Table 1.4 for the values of the main model parameters).

Transport connects the horizontal velocity fields and the rest of the ice properties. SI<sup>3</sup> assumes that the ice properties in the different thickness categories are transported at the same velocity. The scheme of Prather (1986), based on the conservation of 0, 1<sup>st</sup> and 2<sup>nd</sup> order moments in  $x$ - and  $y$ -directions, is used, with

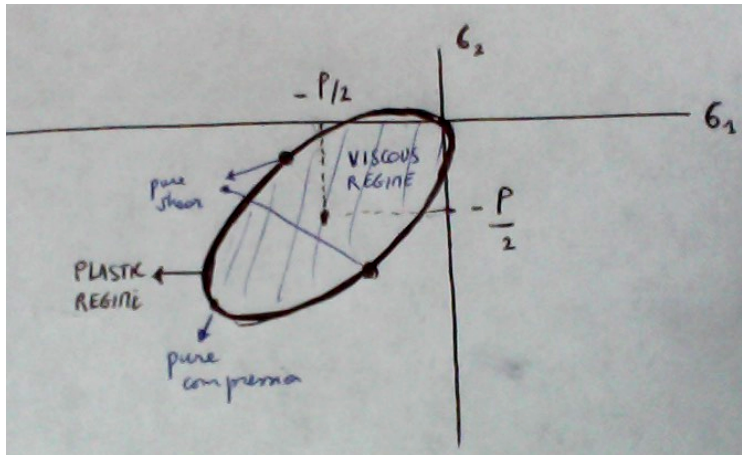


**Figure 1.3:** Elliptical yield curve used in the VP rheologies, drawn in the space of the principal components of the stress tensor ( $\sigma_1$  and  $\sigma_2$ ).

**Table 1.4:** Main model parameters.

	Description	Value	Units	Ref
$P^*$ (rn_pstar)	ice strength thickness param.	20000	N/m <sup>2</sup>	-
$C$ (rn_crhg)	ice strength concentration param.	20	-	(Hibler, 1979)
$H^*$ (rn_hstar)	maximum ridged ice thickness param.	25	m	(Lipscomb et al., 2007)
$p$ (rn_por_rdg)	porosity of new ridges	0.3	-	(Leppäranta et al., 1995)
$amax$ (rn_amax)	maximum ice concentration	0.999	-	-
$h_0$ (rn_hnewice)	thickness of newly formed ice	0.1	m	-

some numerical diffusion if desired. Whereas this scheme is accurate, nearly conservative, it is also quite expensive since, for each advected field, five moments need to be advected, which proves CPU consuming, in particular when multiple categories are used. Other solutions are currently explored.

The dissipation of energy associated with plastic failure under convergence and shear is accomplished by rafting (overriding of two ice plates) and ridging (breaking of an ice plate and subsequent piling of the broken ice blocks into pressure ridges). Thin ice preferentially rafts whereas thick ice preferentially ridges (Tuhkuri and Lensu, 2002). Because observations of these processes are SI<sup>3</sup>ited, their representation in SI<sup>3</sup> is rather heuristic. The amount of ice that rafts/ridges depends on the strain rate tensor invariants (shear and divergence) as in (Flato and Hibler, 1995), while the ice categories involved are determined by a participation function favouring thin ice (Lipscomb et al., 2007). The thickness of ice being deformed ( $h'$ ) determines whether ice rafts ( $h' < 0.75$  m) or ridges ( $h' > 0.75$  m), following Haapala (2000). The deformed ice thickness is  $2h'$  after rafting, and is distributed between  $2h'$  and  $2\sqrt{H^*h'}$  after ridging, where  $H^* = 25$  m

(Lipscomb et al., 2007). Newly ridged ice is highly porous, effectively trapping seawater. To represent this, a prescribed volume fraction (30%) of newly ridged ice (Leppäranta et al., 1995) incorporates mass, salt and heat are extracted from the ocean. Hence, in contrast with other models, the net thermodynamic ice production during convergence is not zero in SI<sup>3</sup>, since mass is added to sea ice during ridging. Consequently, simulated new ridges have high temperature and salinity as observed (Høyland, 2002). A fraction of snow (50 %) falls into the ocean during deformation.

## 1.5 Ice thermodynamics

In this section, we develop the underlying principles of the thermodynamic formulation, summarized in the term  $\Theta^X$ , where  $X$  refers to all extensive state variables.  $\Theta^X$  includes the contributions of transport in thickness space and thermodynamic source and sink terms.

### 1.5.1 Transport in thickness space

Transport in thickness space describes how vertical growth and melt moves ice state variables among the different thicknesses at a velocity  $f(h)$ , the net ice growth/melt rate, which needs to be first computed. In discretized form, this term moves ice properties between neighbouring categories. The linear remapping scheme of Lipscomb et al. (2007) is used. This scheme is semi-lagrangian, second-order, is less diffusive and converges faster than other options.

### 1.5.2 Thermodynamic source and sink terms

Since heat, salt and mass are strongly inter-dependent for sea ice, the thermodynamic source and sink terms are treated together. They include the changes in extensive sea ice state associated with thermodynamic processes. The latter are separated in two main parts: (i) open water fraction processes, where atmosphere and ocean are in direct interaction; and (ii) vertical ice thermodynamic processes, driven by surface snow/ice-atmosphere and basal ice-ocean exchanges, for each thickness category. For each part, first, the energy available or lost is specified. Then the impact on mass exchanges is evaluated. The latter part requires to specify how sea ice and snow responds to energy supply or loss, which is achieved through the enthalpy formulation.

#### Enthalpy formulation

A first overarching aspect of the thermodynamic calculations is the specification of the response of sea ice to energy supply. This is achieved by defining the internal

energy (or enthalpy<sup>5</sup>). This ultimately relies on the response of the phase composition to salinity and temperature changes. The enthalpy formulation used in SI<sup>3</sup> is based on the following assumptions:

- Sea ice is gas-free, composed solely of pure ice and saline brine, characterized by brine fraction  $\phi$ ;
- brine and pure ice are in thermodynamic equilibrium;
- the salinity-dependence of the freezing point is linear (linear liquidus);
- the density of the sea ice (ice+brine) medium is constant ( $\rho_i$ ).

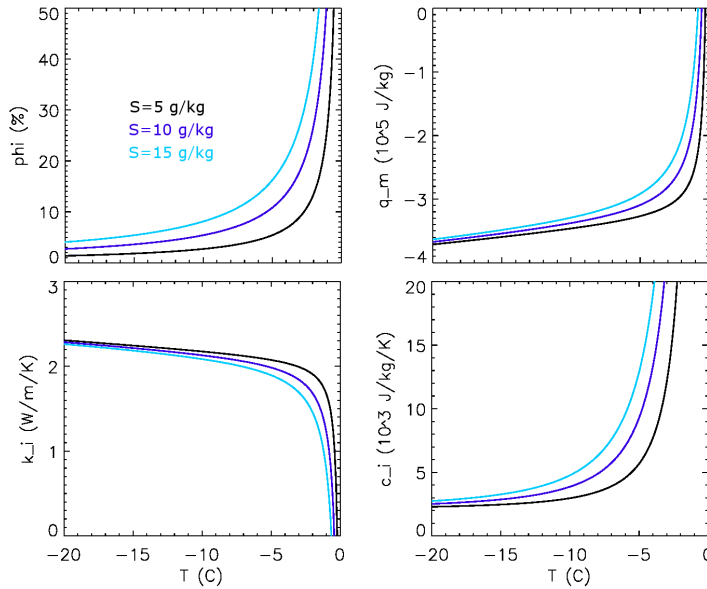


**Figure 1.4:** Thermal properties of sea ice vs temperature for different bulk salinities: brine fraction, specific enthalpy, thermal conductivity, and effective specific heat.

Based on these, brine fraction reduces to  $\phi = -\mu S/T$  (see Fig. 1.4), where  $\mu$  relates the freezing point of brine to salinity, and one can derive the specific enthalpy  $q_m(S, T)$ , defined as the energy required to warm and melt a unit control volume of sea ice at temperature  $T$  (in Celsius) and salinity  $S$  until  $0^\circ\text{C}$ , taken as a reference zero-energy level (Schmidt et al., 2004):

$$q_m(S, T) = \left[ c_i(T + \mu S) - L \left( 1 + \frac{\mu S}{T} \right) - c_w \mu S \right] \quad (1.15)$$

where  $c_i$  is pure ice specific heat,  $L$  is latent heat of fusion at  $0^\circ\text{C}$ , and  $c_w$  is water specific heat. The first term expresses the warming of solid ice. The second term

<sup>5</sup>Wording it internal energy or enthalpy is equivalent since pressure effects are not considered.

expresses internal change in brine fraction, which is often the largest because the Stefan number ( $c_i T/L$ ) is generally small. The last term gives the warming of the remaining water from  $T_{fr} = -\mu S$  until  $0^\circ\text{C}$ . Similar, but simpler and linear expressions for snow and water can be derived.

The second overarching aspect is that all growth and melt processes must be calculated consistently with the enthalpy formulation. Energetics of phase transitions are handled using the formalism of Schmidt et al. (2004). For each phase transition, initial and final states (temperature and salinity) are defined, and the ice-to-ocean mass flux to the ice  $F_m$  (kg/s) relates to the energy gain or loss  $\Delta Q$  through:

$$\Delta Q/\Delta q_m = F_m, \quad (1.16)$$

where  $\Delta q_m$  is the change in specific enthalpy involved in the considered phase transition, from initial to final state.

### Open water processes

As part of the sea ice thermodynamic calculations, a heat budget estimate for the uppermost ocean level ( $B^{opw}$ ) must be included, to compute the rate of new ice formation or the contribution of sensible heat to bottom melting.  $B^{opw}$  includes:

- the absorption of a fraction  $f_1^{qsr}$  of solar radiation (given by radiative transfer component of the ocean model);
- the non-solar heat flux absorbed at the surface;
- the sensible heat content of precipitation
- the sensible heat flux from the ocean to the sea ice ( $A.F_w$ )

Other contributions are not assumed not to contribute. The ocean-to-ice sensible heat flux is formulated the bulk formula of (McPhee, 1992).

If  $B^{opw}$  is such that the SST would decrease below the freezing point, the remainder of the heat is used to form new ice. The heat loss is converted into a volume of new ice  $v_0$ . The thickness  $h_0$  of the new ice grown during a sea ice time step depends on unresolved small-scale currents and waves and is prescribed. The fraction  $a_0 = v_0/h_0$  is computed accordingly. The salinity of this new ice  $S_0$  is given by the salinity-thickness empirical relationship of Kovacs (1996). The temperature assumed for this new ice is the local freezing point. If by contrast  $B^{opw}$  is positive and there still is ice in the grid cell, then  $B^{opw}$  is directly redirected to bottom melting. This argument follows from Maykut and MCPhee (1995), who found that most of solar heat absorbed in the surface waters is converted into melting. In practise, this prevents the SST to be above freezing as long ice is present.

$B^{opw}$  can be seen as a predictor of the heat budget of the first ocean level. As such, it only helps to compute new ice formation and the extra bottom melt in

summer, but is not part of the conservation of heat in the model. To ensure heat conservation, the heat effectively contributing to changing sea ice is removed from the non-solar flux sent to the ocean. This includes: (i) the heat loss used for ice formation, (ii) the heat gain used to melt ice, and (iii) the sensible heat given by the ocean to the ice. Finally, because ice dynamics are not able to maintain the small amount of open water that is observed, a maximum ice fraction (*amax*,  $< 1$ ) is prescribed.

### Vertical ice thermodynamic processes

The second part of the computations regard the computation of purely vertical processes in the ice-covered part of the grid cell, similarly for each ice category.

**Surface melt, basal growth and melt and diffusion of heat.** The surface melt rate, as well as the basal growth / melt rate depend on the energy budget at the upper and lower interfaces, respectively, between the external fluxes either from the atmosphere or the ocean, and the internal conduction fluxes. The internal conduction fluxes depend on the internal temperature profile, which is determined by solving the enthalpy equation:

$$\rho \frac{\partial q_m}{\partial t} = -\frac{\partial}{\partial z}(F_c + F_r). \quad (1.17)$$

which state that the local change in enthalpy is given by the divergence of the vertical conduction ( $F_c = -k(S, T)\partial T/\partial z$ ) and radiation ( $F_r$ ) fluxes.  $\rho$  is the density of ice or snow. Re-expressed as a function of temperature, this becomes the heat diffusion equation. This equation is non-linear in  $T$ , because of  $q$  and  $k$ , and its main specificity is that internal melting requires large amounts of energy near the freezing point. The thermal conductivity is formulated following [Pringle et al. \(2007\)](#), empirically accounting for the reduction of thermal conductivity at large brine fractions.

At the ice base, we assume that the temperature is at the local freezing point. Ice grows or melt if the heat balance between the oceanic sensible heat flux ( $F_w$ ) and internal conduction is negative or positive.

At the ice surface, the boundary condition on the heat diffusion equation is:

$$Q^{sr} + Q^{ns}(T_{su}) = F_c + Q^{sum}. \quad (1.18)$$

where  $Q^{sr}$  and  $Q^{ns}$  are the net downwelling atmospheric solar and non-solar flux components. If the solution of this equation without melting gives a surface temperature ( $T_{su}$ ) below  $0^\circ$  C, then there is no melting and the heat available for surface melting  $Q_{sum} = 0$ . Otherwise  $T_{su}$  is capped at  $0^\circ$  C and  $Q_{sum}$  is calculated as a residual.

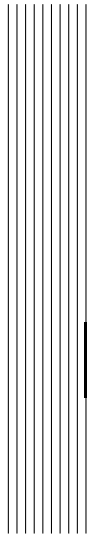
**Radiation.** Radiation contributes to the surface and internal heat budget. The radiative transfer scheme is currently basic, composed of surface albedo, transmission through the ice interior and attenuation with vertical depth. The albedo is

computed empirically as a function of ice thickness, snow depth and surface temperature, using a reformulation of the parameterization of [Shine and Henderson-Sellers \(1985\)](#). When snow is present, all the absorbed radiation is transformed into sensible heat available for conduction or melting. Over snow-free ice, a fraction of solar radiation is transmitted below the surface and attenuates exponentially with depth, until it reaches the base of the ice.

**Growth and melt processes.** Snow grows from precipitation and loses mass from melting and snow-ice conversion once the snow base is below sea level. Sea ice grows and melts by various means. Ice forms by congelation or melt at the base, can melt at the surface and form from snow-to-ice conversion at the snow-ice interface if the latter is below sea level. Some new ice is also added to the system when seawater is trapped into newly formed pressure ridges.

**Salt dynamics.** Bulk salinity is empirically parameterized, as a function of salt uptake during growth, gravity drainage and flushing. The shape of the vertical profile depends on the bulk salinity ([Vancoppenolle et al., 2009b](#)).

**Single-category parameterizations.** If the single-category representation is adopted, then two parameterizations can be activated, following [Fichefet and Morales Maqueda \(1997\)](#). First, the thermal conductivity of both ice and snow is multiplied by a factor  $> 1$  accounting for the unresolved thin ice, effectively increasing the ice growth rate. Second, to account for the loss of thin ice in summer, the ice concentration is reduced in proportion to the loss of ice thickness. Both parameterizations have been tuned to match the results in multi-category mode.



## 2 Time, space and thickness space domain

### Contents

---

<b>2.1 Time domain</b> . . . . .	<b>19</b>
<b>2.2 Spatial domain</b> . . . . .	<b>20</b>
<b>2.3 Thickness space domain</b> . . . . .	<b>21</b>

---

Having defined the model equations in previous Chapter, we need now to choose the numerical discretization. In the present chapter, we provide a general description of the SI<sup>3</sup> discretization strategy, in terms of time, space and thickness, which is considered as an extra independent variable.

Sea ice state variables are typically expressed as:

$$X(ji, jj, jk, jl). \tag{2.1}$$

*ji* and *jj* are x-y spatial indices, as in the ocean. *jk* = 1, ..., *nlay\_i* corresponds to the vertical coordinate system in sea ice (ice layers), and only applies to vertically-resolved quantities (ice enthalpy and salinity). *jl* = 1, ..., *jpl* corresponds to the ice categories, discretizing thickness space.

### 2.1 Time domain

The sea ice time stepping is synchronized with that of the ocean. Because of the potentially large numerical cost of sea ice physics, in particular rheology, SI<sup>3</sup> can be called every *nn\_fsbc* time steps (*namsbc* in *namelist\_ref*). The sea ice time step is therefore *rdt\_ice* = *rdt* \* *nn\_fsbc*. In terms of quality, the best value for *nn\_fsbc*

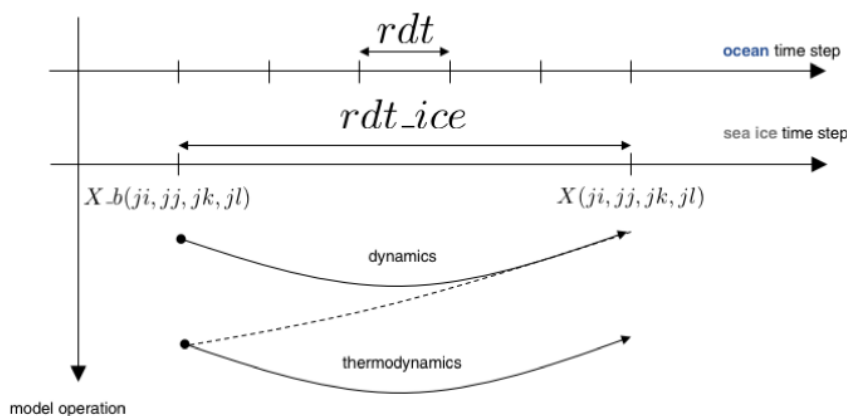


**Figure 2.1:** Schematic representation of time stepping in SI<sup>3</sup>, assuming  $nn\_fsc = 5$ .

is 1, providing full consistency between sea ice and oceanic fields. Larger values (typically 2 to 5) can be used but numerical instabilities can appear because of the progressive decoupling between the state of sea ice and that of the ocean, hence changing  $nn\_fsc$  must be done carefully.

Ice dynamics (rheology, advection, ridging/rafting) and thermodynamics are called successively. To avoid pathological situations, thermodynamics were chosen to be applied on fields that have been updated by dynamics, in a somehow semi-implicit procedure.

There are a few iterative / subcycling procedures throughout the code, notably for rheology, advection, ridging/rafting and the diffusion of heat. In some cases, the arrays at the beginning of the sea ice time step are required. Those are referred to as  $X_b$ .

## 2.2 Spatial domain

The horizontal indices  $ji$  and  $jj$  are handled as for the ocean in NEMO, assuming C-grid discretization and in most cases a finite difference expression for scale factors.

The vertical index  $jk = 1, \dots, nlay\_i$  is used for enthalpy (temperature) and salinity. In each ice category, the temperature and salinity profiles are vertically resolved over  $nlay\_i$  equally-spaced layers. The number of snow layers can currently only be set to  $nlay\_s = 1$  (Fig. 2.2).

To increase numerical efficiency of the code, the two horizontal dimensions of an array  $X(ji, jj, jk, jl)$  are collapsed into one (array  $X\_1d(ji, jk, jl)$ ) for thermodynamic computations, and re-expanded afterwards.

```
!-----
&nampar          !   Generic parameters
```

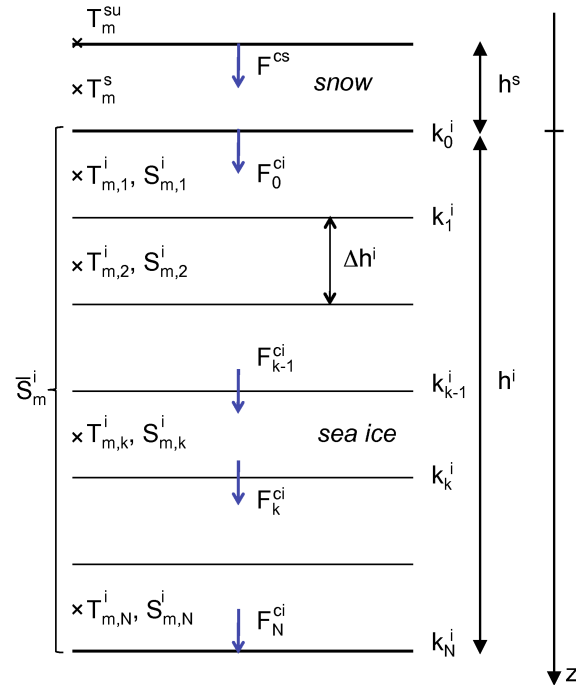


**Figure 2.2:** Vertical grid of the model, used to resolve vertical temperature and salinity profiles

```

!-----
jpl          = 5           ! number of ice categories
nlay_i      = 2           ! number of ice layers
nlay_s      = 2           ! number of snow layers
ln_virtual_itd = .false.  ! virtual ITD mono-category
  ↪ parameterization (jpl=1 only)
!           ! i.e. enhanced thermal
  ↪ conductivity & virtual thin
  ↪ ice melting

ln_icedyn   = .true.      ! ice dynamics (T) or not (F)
ln_icethd   = .true.      ! ice thermo (T) or not (F)
rn_amax_n   = 0.997       ! maximum tolerated ice
  ↪ concentration NH
rn_amax_s   = 0.997       ! maximum tolerated ice
  ↪ concentration SH

```

## 2.3 Thickness space domain

```

!-----
&namitd      ! Ice discretization
!-----
ln_cat_hfn   = .true.     ! ice categories are defined by a
  ↪ function following rn_himean**(-0.05)

```

```

rn_himean      = 2.0           ! expected domain-average ice
  ↳ thickness (m)
ln_cat_usr     = .false.      ! ice categories are defined by
  ↳ rn_catbnd below (m)
rn_catbnd     = 0.,0.45,1.1,2.1,3.7,6.0
rn_himin      = 0.1           ! minimum ice thickness (m) allowed

```

Thickness space is discretized using  $j_l = 1, \dots, j_{pl}$  thickness categories, with prescribed boundaries  $hi\_max(j_l - 1), hi\_max(j_l)$ . Following Lipscomb (2001), ice thickness can freely evolve between these boundaries. The number of ice categories  $j_{pl}$  can be adjusted from the namelist (*nampar*).

There are two means to specify the position of the thickness boundaries of ice categories. The first option (*ln\_cat\_hfn*) is to use a fitting function that places the category boundaries between 0 and  $3\bar{h}$ , with  $\bar{h}$  the expected mean ice thickness over the domain (namelist parameter *rn\_himean*), and with a greater resolution for thin ice (Fig. 2.3). More specifically, the upper limits for ice in category  $j_l = 1, \dots, j_{pl} - 1$  are:

$$hi\_max(j_l) = \left( \frac{j_l \cdot (3\bar{h} + 1)^\alpha}{(j_{pl} - j_l)(3\bar{h} + 1)^\alpha + j_l} \right)^{\alpha^{-1}} - 1, \quad (2.2)$$

with  $hi\_max(0)=0$  m and  $\alpha = 0.05$ . The last category has no upper boundary, so that it can contain arbitrarily thick ice.

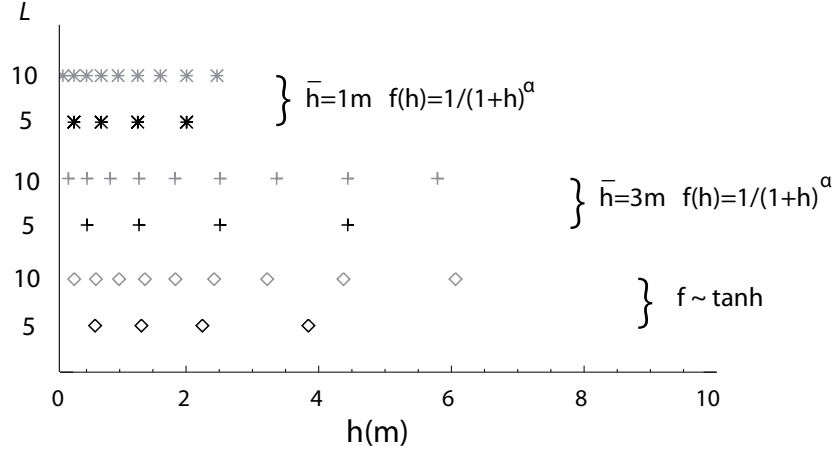


**Figure 2.3:** Boundaries of the model ice thickness categories (m) for varying number of categories and prescribed mean thickness ( $\bar{h}$ ). The formerly used *tanh* formulation is also depicted.

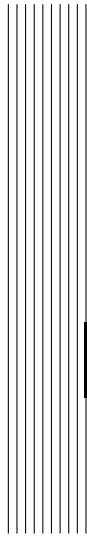
The other option (*ln\_cat\_usr*) is to specify category boundaries by hand using *rn\_catbnd*. The first category must always be thicker than *rn\_himin* (0.1 m by default).

The choice of ice categories is important, because it constraints the ability of the model to resolve the ice thickness distribution. The latest study (Massonnet

et al., 2019) recommends to use at least 5 categories, which should include one thick ice with lower bounds at  $\sim 4$  m and  $\sim 2$  m for the Arctic and Antarctic, respectively, for allowing the storage of deformed ice.

With a fixed number of cores, the cost of the model linearly increases with the number of ice categories. Using  $jpl = 1$  single ice category is also much cheaper than with 5 categories, but seriously deteriorates the ability of the model to grow and melt ice. Indeed, thin ice thicknes faster than thick ice, and shrinks more rapidly as well. When `nn_virtual_itd=1` ( $jpl = 1$  only), two parameterizations are activated to compensate for these shortcomings. Heat conduction and areal decay of melting ice are adjusted to closely approach the 5 categories case.





## 3 Ice dynamics

### Contents

---

<b>3.1 Representation of sea ice drift in <math>SI^3</math></b> . . . . .	<b>26</b>
3.1.1 Basal stress and landfast sea ice . . . . .	27
3.1.2 Ice strength and tensile strength . . . . .	27
3.1.3 Namelist parameters . . . . .	27
<b>3.2 The interaction force, deformation, internal stresses</b> . . . . .	<b>27</b>
<b>3.3 The viscous-plastic (VP) line-successive relaxation (LSR) solver</b> . . . . .	<b>30</b>
3.3.1 The VP rheology . . . . .	30
3.3.2 The LSR numerical approach . . . . .	30
<b>3.4 EVP solvers</b> . . . . .	<b>32</b>
<b>3.5 The EAP solver</b> . . . . .	<b>32</b>
3.5.1 The EAP rheology . . . . .	32
3.5.2 The EAP solver . . . . .	32

---

*Dynamics* in the sea ice world refer to the horizontal drift of sea ice in response to winds, ocean currents and Earth's rotation.

In SI<sup>3</sup>, as in virtually all sea ice models, sea ice drift is represented assuming sea ice is a 2D continuum characterized by a Eulerian 2D velocity field  $\mathbf{u} = (u, v)$ , solution of the conservation of linear momentum, with wind stress, ocean current velocity, and sea surface tilt as external forcings.

The sea ice continuum is assumed non-newtonian: internal stresses do not linearly relate to deformation; a so-called *rheology* characterizes this relationship. Strong non-linearities in the rheology render the numerical resolution of the momentum equation challenging.

In SI<sup>3</sup> there are three numerical solvers for the momentum equation. Each corresponds to a specific rheological model: a viscous-plastic (VP) rheology, solved either with a line successive relaxation technique (LSR) or with the elastic-viscous-plastic (EVP) approach; and an elastic-anisotropic-plastic (EAP) rheology.

The important namelist options relate to:

- the type of sea ice rheology used;
- the parameters controlling the often slow numerical convergence of the solver;
- other options related to relatively new physical add-ons, such as basal stress or tensile strength.

In this chapter we describe how sea ice drift is represented in SI<sup>3</sup>. First, we give some general information on the represented physics of sea ice drift. Second, we focus on interaction forces, deformation and sea ice stresses. Three, we detail the three different rheological formulations in SI<sup>3</sup>.

### 3.1 Representation of sea ice drift in SI<sup>3</sup>

The 2D linear momentum equation for sea ice velocity reads:

$$m \frac{\partial \mathbf{u}}{\partial t} = A (\boldsymbol{\tau}_a + \boldsymbol{\tau}_w) + \boldsymbol{\tau}_b - m f \mathbf{k} \times \mathbf{u} - mg \nabla \eta + \nabla \cdot \boldsymbol{\sigma}, \quad (3.1)$$

Acceleration on the left-hand side is the sum of atmospheric, oceanic, basal, Coriolis, sea-surface tilt and internal stresses. A few general remarks:

- momentum advection is neglected;
- the mass per unit area  $m$  is a multi-category average including open water of the weight of snow and ice, and does not change during momentum transfer;
- wind and ice-ocean stresses  $\boldsymbol{\tau}_a$  and  $\boldsymbol{\tau}_w$  are weighted by ice concentration  $A$  to ensure zero stress for nil ice cover (Connolley et al., 2004)

- wind stress is assumed constant during time step
  - the ice-ocean stress scales like  $u - u_{oce}^2$ , where  $u_{oce}$  is the average ocean current ? over the previous nn\_fsbc time steps ?
  - the Coriolis factor is given at T-point and depends on latitude ( $f = 2 \Omega \sin \phi$ )
  - sea surface height is an average of value at previous time step
  - basal stress has recently been added to enable the emergence of landfast sea ice
  - internal force is tricky and has a dedicated section
- !!! Boundary conditions can be free-slip or no-slip

### 3.1.1 Basal stress and landfast sea ice

Basal stress parameterizations

### 3.1.2 Ice strength and tensile strength

Ice strength

Tensile strength

### 3.1.3 Namelist parameters

table with some namelist parameters

## 3.2 The interaction force, deformation, internal stresses

The internal interaction force per unit area ( $\text{N/m}^2$ ) is given by:

$$\mathbf{F} \equiv \nabla \cdot \boldsymbol{\sigma}, \quad (3.2)$$

where  $\boldsymbol{\sigma}$  is the integral of the Cauchy stress tensor through the depth of the ice (here after stress tensor,  $\text{N/m}$ ). Interaction force is one of the key terms in the momentum equation and is the most physically and numerically challenging.

For solids, including sea ice, internal stress (caused by floe-floe or floe-lead interactions) depend on deformation, the material properties of sea ice, and the state of the ice cover, which is known as sea ice rheology (Feltham, 2008).

Rheological models for sea ice are complicated and possibly inadequate at small scales. Because of this, they have been a long subject of debate in the community (Blockley et al., 2020). In SI<sup>3</sup> we include several solvers for the momentum equation, corresponding to various rheologies. All require some background elements on deformation and stress which we give in this section.

### Deformation

The deformation state of sea ice plays a central role in the interaction force. The (E)VP rheological models relate internal stress to strain rate, which can be characterized by the strain rate tensor:

$$\dot{\epsilon}_{ij} \equiv \frac{1}{2} \left( \frac{\partial u_i}{\partial x_j} + \frac{\partial u_j}{\partial x_i} \right). \quad (3.3)$$

We follow [Hunke and Dukowicz \(2002\)](#) and introduce divergence, tension and shear strain rates, which facilitate the use of orthogonal curvilinear coordinates:

$$\dot{\epsilon}_1 = \dot{\epsilon}_{11} + \dot{\epsilon}_{22} \equiv D_D \quad (3.4)$$

$$\dot{\epsilon}_2 = \dot{\epsilon}_{11} - \dot{\epsilon}_{22} \equiv D_T, \quad (3.5)$$

$$2\dot{\epsilon}_{12} \equiv D_S. \quad (3.6)$$

On the Arakawa C-grid used in NEMO, the diagonal terms of the strain rate tensor (equivalently  $D_D$  and  $D_T$ ) are most useful at  $T$ -points and the symmetric off-diagonal term (equivalently  $D_S$ ) at  $F$ -points. Their discrete form is (assuming an orthogonal curvilinear system):

$$\begin{aligned} D_D &= \frac{1}{e_{1t}e_{2t}} (\delta_i[e_{2u}u] + \delta_j[e_{1v}v]), \\ D_T &= \frac{1}{e_{1t}e_{2t}} \left( e_{2t}^2 \delta_i \left[ \frac{u}{e_{2u}} \right] - e_{1t}^2 \delta_j \left[ \frac{v}{e_{1v}} \right] \right), \\ D_S &= \frac{1}{e_{1f}e_{2f}} \left( e_{1f}^2 \delta_{j+1/2} \left[ \frac{u}{e_{1u}} \right] + e_{2f}^2 \delta_{i+1/2} \left[ \frac{v}{e_{2v}} \right] \right). \end{aligned} \quad (3.7)$$

Maximum shear rate, required in SIMIP diags, can be defined as the second strain rate tensor invariant  $\epsilon_{II} = \sqrt{D_T^2 + D_S^2}$ , and should not be confused with (pure) shear ( $D_S$ ).

### Internal stresses and interaction force

The 2-D stress tensor

$$\boldsymbol{\sigma} = \begin{pmatrix} \sigma_{11} & \sigma_{12} \\ \sigma_{12} & \sigma_{22} \end{pmatrix} \quad (3.8)$$

has by construction equal off-diagonal elements. The following combinations (here referred to as *sea ice stresses*):

$$\begin{aligned} \sigma_1 &= \sigma_{11} + \sigma_{22}, \\ \sigma_2 &= \sigma_{11} - \sigma_{22}. \end{aligned} \quad (3.9)$$

are used in SI3, together with  $\sigma_{12}$  ([Hunke and Dukowicz, 2002](#); [Bouillon et al., 2013](#)), as they simplify the rheological equations in curvilinear orthogonal coordinates.

The interaction force components are given by the divergence of the stress tensor. The divergence of a tensor in curvilinear orthogonal coordinates comes out of tensor analysis, which according to [Hunke and Dukowicz \(2002\)](#) is *complex and intimidating*. In their paper the continuous expression is given, and here we only give the discrete form:

$$\begin{aligned} F_u &\equiv \frac{1}{2 e_{1u} e_{2u}} \left[ e_{2u} \partial_i \sigma_1 + \frac{1}{e_{2u}} \partial_i (e_{2t}^2 \sigma_2) + \frac{2}{e_{1u}} \partial_j (e_{1f}^2 \sigma_{12}) \right], \\ F_v &\equiv \frac{1}{2 e_{1v} e_{2v}} \left[ e_{1v} \partial_j \sigma_1 - \frac{1}{e_{1v}} \partial_j (e_{1t}^2 \sigma_2) + \frac{2}{e_{2v}} \partial_i (e_{2f}^2 \sigma_{12}) \right]. \end{aligned} \quad (3.10)$$

### Standard stress diagnostics

Stress tensor invariants (for SIMIP diagnostics) and principal stresses (elliptical yield curve check) are also useful. The principal stresses (here  $\sigma_1^p, \sigma_2^p$ ) are given by diagonalisation of the stress tensor:

$$\sigma_{1,2}^p = \frac{\sigma_{11} + \sigma_{22}}{2} \pm \sqrt{\left(\frac{\sigma_{11} - \sigma_{22}}{2}\right)^2 + \sigma_{12}^2}. \quad (3.11)$$

One can easily retrieve these  $\sigma_{\mathbf{x}_i} = \sigma_i^p \cdot \mathbf{x}_i$  where  $x_i$  are eigenvectors. Expressed in terms of sea ice stresses, principal stresses read:

$$\sigma_{1,2}^p = \frac{\sigma_1}{2} \pm \sqrt{\left(\frac{\sigma_2}{2}\right)^2 + \sigma_{12}^2} \quad (3.12)$$

Two invariants of the stress tensor are also often introduced ([Coon et al., 1974](#); [Feltham, 2008](#); [Notz et al., 2016](#)), which are useful as they do not change with the coordinate system:

$$\sigma_{1,2}^p \equiv \sigma_I \pm \sigma_{II}. \quad (3.13)$$

$\sigma_I$  is also referred to as *negative pressure* or *averaged normal stress*, whereas  $\sigma_{II}$  is referred to as the *maximum shear stress*.

Expressed in terms of sea ice stresses, the stress tensor invariants read as:

$$\begin{aligned} \sigma_I &= \sigma_1/2, \\ \sigma_{II} &= \sqrt{\sigma_2^2/4 + \sigma_{12}^2}. \end{aligned} \quad (3.14)$$

Stress invariants can also be expressed in terms of principal stresses:

$$\begin{aligned} \sigma_I &= \frac{\sigma_1^p + \sigma_2^p}{2}, \\ \sigma_{II} &= \frac{\sigma_1^p - \sigma_2^p}{2}. \end{aligned} \quad (3.15)$$

To plot the yield curve ([Lemieux and Dupont, 2020](#)), e.g. the charge ellipse for the VP rheology, one needs to  $\sigma_2^p/P$  vs  $\sigma_1^p/P$ .

### 3.3 The viscous-plastic (VP) line-successive relaxation (LSR) solver

#### 3.3.1 The VP rheology

The viscous-plastic (VP) rheology implemented in SI3 (activated by `ln_rhg_vp`) essentially follows [Zhang and Hibler \(1997\)](#); [Lemieux and Tremblay \(2009\)](#); [Losch et al. \(2010\)](#) and resolves the momentum equation assuming a viscous plastic rheology:

$$\begin{aligned}\sigma_1 &= \frac{P}{\Delta^*} (D_D - \Delta), \\ \sigma_2 &= \frac{P}{e^2 \Delta^*} D_T, \\ \sigma_{12} &= \frac{P}{2 e^2 \Delta^*} D_S.\end{aligned}\tag{3.16}$$

$\Delta = \sqrt{D_D^2 + e^{-2}(D_T^2 + D_S^2)}$  is a measure of total deformation, particular to the VP model, used to equally partition viscous stresses into the yield curve [Hibler \(1979\)](#).

Using  $\Delta^* = \Delta + \Delta_{min}$  ensures the model is differentiable [Bouillon et al. \(2013\)](#).  $\Delta_{min}$  (`rn_creepI`) is a parameter that constrains viscous flow to small deformations and must be kept as small as possible.

$P$  is the sea ice strength (N/m), for which we use  $P = P^* \cdot h \cdot \exp[-C(1 - A)]$  ([Hibler, 1979](#)).  $P^*$  (`rn_pstar`) and  $C$  (`rn_crhg`) are two tuning parameters.

In the formulation presented above, we use the so-called *replacement pressure*  $P \cdot \Delta / \Delta^*$ , i.e., we assume sea ice strength ( $P$ ) and (replacement) pressure are distinct, which avoids residual stress and drift for zero deformation [Lemieux and Dupont \(2020\)](#).

#### 3.3.2 The LSR numerical approach

The internal forces introduce the key challenges to solve the momentum equations:

$$\begin{aligned}(m^n / \Delta t) \cdot (u^{n+1} - u^n) &= \sum F_u^{n+1}, \\ (m^n / \Delta t) \cdot (v^{n+1} - v^n) &= \sum F_v^{n+1}.\end{aligned}\tag{3.17}$$

where we seek solutions at time step  $n + 1$  for known forcing and velocities at time step  $n$ , treating all forces implicitly. A key steps to solution [Zhang and Hibler \(1997\)](#) are, for the U- (V-) equation, (i) to sort all u- (v-) dependent terms in the left hand-side (LHS) and all other terms in the right-hand side (RHS); (ii) to treat all terms implicitly in time, leading to:

$$\begin{aligned}A^U(\mathbf{u}^c) \cdot u^{k+1} &= \text{RHS}^U(v^c), \\ A^V(\mathbf{u}^c) \cdot v^{k+1} &= \text{RHS}^V(u^c),\end{aligned}\tag{3.18}$$

where  $A^X$  are tridiagonal matrices,  $RHS^X$  are vectors. As the system of equation is coupled and non-linear, the solution must be iterated, and for a large number of *outer* iterations  $k$ ,  $\mathbf{u}^k$  should converge to solution at time step  $n + 1$ . To improve stability, previous authors have suggested to replace  $\mathbf{u}_k$  by its average over past two iterates  $\mathbf{u}^c = 0.5 \cdot (\mathbf{u}^{k-1} + \mathbf{u}^k)$ .

The spatial discretization leads to a system of linear equations for  $u^{k+1}$  and  $v^{k+1}$ , of the kind

$$AU_{ij}u_{i-1,j}^{k+1} + BU_{ij}u_{i,j}^{k+1} + CU_{ij}u_{i+1,j}^{k+1} = DU_{ij}u_{i,j-1}^{k+1} + EU_{ij}u_{i,j+1}^{k+1} + FU_{ij}. \quad (3.19)$$

where the system coefficients (AU, BU, ...) combine contributions from all forces. The system of  $u$  and  $v$  equations is solved using a *line successive relaxation* technique (LSR) requiring an additional (*inner*) 2-step iteration level, fairly close in essence to that of [Zhang and Hibler \(1997\)](#).

We start by treating  $u$  along each line  $j$ . Step 1 is to use the Thomas algorithm for tridiagonal systems of equations, using previous iterate values for velocities in the  $j+1$  and  $j-1$  lines in the right-hand side, giving  $u_1$ . In a second step,  $u_1$  is merged (say *relaxed*) to previous iterate value, giving  $u_2 = u_1 + w \cdot (u_1 - u_0)$ , where  $0 < w < 2$  is called the relaxation coefficient (rn\_relaxu\_vp).  $u_2$  is then substituted into  $u$ , in order to propagate information to the next line. Once  $u$  is obtained over all lines of the domain (from south to north), the procedure is repeated for  $v$ , but along columns. We left the possibility for  $v$  to have its own relaxation coefficient (rn\_relaxv\_vp). At convergence (decided from tolerance, namelist parameters rn\_uerr\_min\_vp and rn\_verr\_min\_vp), the procedure stops. Once the linear system converges, a new *outer* iteration can start, and velocities are updated into the right hand side. There is also an option to process the solution every odd then every even line / column (ln\_zebra\_vp), which can be helpful to accelerate convergence.

The number of iterations in the two levels of loops is resolution-dependent and must be carefully adjusted to achieve a proper solution (namelist parameters nn\_ninn\_vp and nn\_nout\_vp). They also drastically affect computing time. Typical values at  $2^\circ$  are (TABLE)

### Acceleration, external and Coriolis stresses

Acceleration is divided into LHS ( $mu^{n+1}/\Delta t$ ) and RHS ( $mu^n/\Delta t$ ) contributions. Atmospheric stresses are calculated explicitly at U and V points, and integrated into the RHS, without updating ice velocities, following previous authors. Oceanic stress contributes to LHS ( $= C_d(|\mathbf{u}_c - \mathbf{u}_o|) \cdot u^{k+1}$ ) and RHS ( $= C_d(|\mathbf{u}_c - \mathbf{u}_o|) \cdot u_{oce}$ ), where drag coefficient is treated implicitly (i.e. as a function of  $\mathbf{u}_c$ ). Coriolis contributes to RHS only and is also treated implicitly. Finally, the sea surface tilt term is explicit.

### Tridiagonal solver and relaxation

$$\mathbf{u}^{k+1} = \mathbf{u}^k + \omega \cdot (\mathbf{u}^{k+1} - \mathbf{u}^k) \quad (3.20)$$

### 3.4 EVP solvers

Including aEVP

### 3.5 The EAP solver

#### 3.5.1 The EAP rheology

The (Elastic-)Anisotropic-Plastic (EAP) rheology was developed by Wilchinsky and Feltham [Wilchinsky et al. \(2006\)](#) and implemented in CICE by Tsamados et al., who added the elastic component for numerical reasons [Tsamados et al. \(2013\)](#). The SI3 implementation is adapted from the CICE code. EAP is a continuum rheology for pack ice. It assumes sea ice consists of identical diamond shaped floes, the top angle of which is a tuning parameter. The relative orientation of floes is changeable, giving rise to the structure tensor  $A$  describing the degree of anisotropy resulting from aligned floes. Alignment results in preferential directions for ridging and sliding changing the VP yield curve into a 3D yield surface.

#### 3.5.2 The EAP solver

The EAP code is subcycled in the same way as the EVP rheology, making  $nn_{evp}$  a common parameter. The evolution of the structure tensor adds two extra equations to be solved during the subcycling. The yield surface depends on the structure tensor and the orientation of the structure tensor versus the strain rate tensor and consequently also needs to be updated within the subcycling.

## 4 Ice transport

### Contents

---

<b>4.1 Second order moments conserving (Prather 1986) scheme</b> <i>(ln_adv_Pra)</i> . . . . .	<b>34</b>
<b>4.2 5<sup>th</sup> order flux-corrected transport scheme (UM5)</b> . . . . .	<b>34</b>

---

```
-----  
&namdyn_adv      !   Ice advection  
!-----  
ln_adv_Pra       = .true.           ! Advection scheme (Prather)  
ln_adv_UMx       = .false.          ! Advection scheme (Ultimate-Macho)  
nn_UMx          = 5                 ! order of the scheme for UMx  
    ↪ (1-5 ; 20=centered 2nd order)
```

**Listing 1:** SI3 namelist, section advection

This section focuses on how LIM solves the advection of ice extensive properties:

$$\frac{\partial X}{\partial t} = -\nabla \cdot (\mathbf{u}X) \quad (4.1)$$

where  $X = X(t, \mathbf{x}, h)$  refers to any global sea ice state variable.

As soon as ice dynamics are activated (`ln_dyn_ALL`), all extensive state variables are to be advected following the horizontal velocity field.

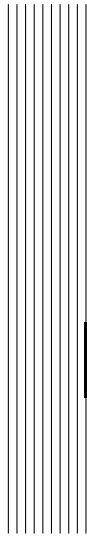
There are two variants of advection calculation: the second-order moment conserving scheme of Prather (1986) (`ln_adv_Pra`) and the Ultimate-Macho (UM) (`ln_adv_UMx`) scheme of arbitrary order (`nn_UMx`).

#### 4.1 Second order moments conserving (Prather 1986) scheme (*In adv Pra*)

The scheme of Prather (1986) explicitly computes the conservation of second-order moments of the spatial distribution of global sea ice state variables. This scheme preserves positivity of the transported variables and is practically non-diffusive. It is also computationally expensive, however it allows to localize the ice edge quite accurately. As the scheme is conditionally stable, the time step is split into two parts if the ice drift is too fast, based on the CFL criterion.

State variables per unit grid cell area are first multiplied by grid cell area. Then, for each state variable, the  $0^{th}$  (mean),  $1^{st}$  ( $x, y$ ) and  $2^{nd}$  ( $xx, xy, yy$ ) order moments of the spatial distribution are transported. At 1st time step, all moments are zero (if prescribed initial state); or read from a restart file, and then evolve through the course of the run. Therefore, for each global variable, 5 additional tracers have to be kept into memory and written in the restart file, which significantly increases the required memory. Advection following  $x$  and  $y$  are computed independently. The succession order of  $x$ - and  $y$ - advection is reversed every time step.

#### 4.2 $5^{th}$ order flux-corrected transport scheme (UM5)



# 5 Ridging and rafting

## Contents

---

<b>5.1 Theory</b>	<b>37</b>
5.1.1 Dynamical inputs	37
5.1.2 The two deformation modes: ridging and rafting	38
5.1.3 Participation functions	38
5.1.4 Transfer functions	39
5.1.5 Ridging shift	40
5.1.6 Mechanical redistribution for other global ice variables	41

---

This chapter focuses on how SI3 solves ridging and rafting:

$$\frac{\partial X}{\partial t} = \Psi^X, \tag{5.1}$$

where  $X$  refers to any global sea ice state variable.

Divergence and shear open the ice pack and create ice of zero thickness. Convergence and shear consumes thin ice and create thicker ice by mechanical deformation. The redistribution functions  $\Psi^X$  describe how opening and mechanical deformation redistribute the global ice state variables into the various ice thickness categories.

The fundamental redistribution function is  $\Psi^g$ , which accounts for area redistribution. The other redistribution functions  $\Psi^X$  associated with other state variables will derive naturally. The redistribution function  $\Psi^g$  should first ensure area conservation. By integrating the evolution equation for  $g(h)$  over all thicknesses,

```

!-----
&namdyn_rdgrft ! Ice ridging/rafting
!-----
      ! -- ice_rdgrft_strength -- !
ln_str_H79      = .true.           ! ice strength param.: Hibler_79
  ↪ => P = pstar*<h>*exp(-c_rhg*A)
  rn_pstar      = 2.0e+04          ! ice strength thickness
    ↪ parameter [N/m2]
  rn_crhg       = 20.0             ! ice strength conc. parameter
    ↪ (-)
ln_str_R75      = .false.          ! ice strength param.: Rothrock_75
  ↪ => P = fn of potential energy
  rn_pe_rdg     = 17.0             ! coef accouting for frictional
    ↪ dissipation
ln_str_CST      = .false.          ! ice strength param.: Constant
  rn_str        = 0.0              ! ice strength value
ln_str_smooth   = .true.          ! spatial smoothing of the ice
  ↪ strength
      ! -- ice_rdgrft -- !
ln_distf_lin    = .true.           ! redistribution function of ridged
  ↪ ice: linear (Hibler 1980)
ln_distf_exp    = .false.          ! redistribution function of ridged
  ↪ ice: exponential => not coded yet
  rn_murdbg     = 3.0              ! e-folding scale of ridged ice
    ↪ (m**.5)
rn_csrdg       = 0.5              ! fraction of shearing energy
  ↪ contributing to ridging
      ! -- ice_rdgrft_prep -- !
ln_partf_lin    = .false.          ! Linear ridging participation
  ↪ function (Thorndike et al, 1975)
  rn_gstar      = 0.15            ! fractional area of thin ice
    ↪ being ridged
ln_partf_exp    = .true.          ! Exponential ridging participation
  ↪ function (Lipscomb, 2007)
  rn_astar      = 0.03            ! exponential measure of ridging
    ↪ ice fraction [set to 0.05 if hstar=100]
ln_ridging     = .true.           ! ridging activated (T) or not (F)
  rn_hstar      = 25.0            ! determines the maximum
    ↪ thickness of ridged ice [m] (Hibler, 1980)
  rn_porordg    = 0.3             ! porosity of newly ridged ice
    ↪ (Lepparanta et al., 1995)
  rn_fsnwrdg    = 0.5             ! snow volume fraction that
    ↪ survives in ridging
  rn_fpndrdg    = 1.0             ! pond fraction that survives in
    ↪ ridging (small a priori)
ln_rafting     = .true.           ! rafting activated (T) or not (F)
  rn_hraft      = 0.75           ! threshold thickness for
    ↪ rafting [m]
  rn_craft      = 5.0             ! squeezing coefficient used in
    ↪ the rafting function
  rn_fsnwrft    = 0.5             ! snow volume fraction that
    ↪ survives in rafting
  rn_fpndrft    = 1.0             ! pond fraction that survives in
    ↪ rafting (0.5 a priori)

```

**Listing 2:** SI3 namelist, section ridging and rafting

recalling that  $\int_0^\infty g(h) = 1$ , and that the total areal change due to thermodynamics

must be zero, e.g.  $\int_0^\infty \partial(fg)/\partial h = 0$ , then the area conservation reads:

$$\int_0^\infty h\Psi^g dh = \nabla \cdot \mathbf{u}. \quad (5.2)$$

Second, we must say something about volume conservation, and this will be done more specifically later. Following [Thorndike et al. \(1975\)](#), we separate the  $\Psi^X$ 's into **(i)** *dynamical inputs*, **(ii)** *participation functions*, i.e., how much area of ice with a given thickness participates to mechanical deformation **(iii)** *transfer functions*, i.e., where in thickness space the ice is transferred after deformation.

## 5.1 Theory

### 5.1.1 Dynamical inputs

A general expression of  $\Psi^g$ , the mechanical redistribution function associated to the ice concentration, was proposed by [Thorndike et al. \(1975\)](#):

$$\Psi^g = |\dot{\epsilon}|[\alpha_o(\theta)\delta(h) + \alpha_d(\theta)w_d(h, g)], \quad (5.3)$$

which is convenient to separate the dependence in  $\mathbf{u}$  from those in  $g$  and  $h$ . The first and second terms on the right-hand side correspond to opening and deformation, respectively.  $|\dot{\epsilon}| = (\dot{\epsilon}_I^2 + \dot{\epsilon}_{II}^2)^{1/2}$ , where  $\dot{\epsilon}_I = \nabla \cdot \mathbf{u}$  and  $\dot{\epsilon}_{II}$  are the strain rate tensor invariants;  $\theta = \text{atan}(\dot{\epsilon}_{II}/\dot{\epsilon}_I)$ .  $w_d(h, g)$ , the deformation mode will be discussed in the next section.  $|\dot{\epsilon}|\alpha_o$  and  $|\dot{\epsilon}|\alpha_d$  are called the lead opening and closing rates, respectively.

The **dynamical** inputs of the mechanical redistribution in  $\text{SI}^3$  are:

- $|\dot{\epsilon}|\alpha_o$ , the opening rate,
- $|\dot{\epsilon}|\alpha_d$ , the net closing rate.

Following [Thorndike et al. \(1975\)](#), we choose  $\int_0^\infty w_d(h, g) dh = -1$ . In order to satisfy area conservation, the relation  $|\dot{\epsilon}|\alpha_o - |\dot{\epsilon}|\alpha_d = \nabla \cdot \mathbf{u}$  must be verified. In the model, there are two ways to compute the divergence of the velocity field. A first way is to use the velocity components ( $\dot{\epsilon}_I = \nabla \cdot \mathbf{u}^{\text{rhg}}$ ) as computed after the rheology (superscript *rhg*). Another way is to derive it from the horizontal transport of ice concentration and open water fraction. In principle, the equality  $A^o + \sum_{l=1}^L g_L^i = 1$  should always be verified. However, after ice transport (superscript *trp*), this is not the case, and one can diagnose a velocity divergence using the departure from this equality:  $\nabla \cdot \mathbf{u}^{\text{trp}} = (1 - A^o - \sum_{l=1}^L g_L^i)/\Delta t$ . In general, we will use  $\dot{\epsilon}_I$  unless otherwise stated.

The **net closing rate** is written as a sum of two terms representing the energy dissipation by shear and convergence ([Flato and Hibler, 1995](#)):

$$|\dot{\epsilon}|\alpha_d(\theta) = C_s \frac{1}{2} (\Delta - |\dot{\epsilon}_I|) - \min(\dot{\epsilon}_I, 0), \quad (5.4)$$

where  $\Delta$  is a measure of deformation (defined in the rheology section). The factor  $C_s = 0.5$  ( $C_s$  in *namelist\_ice*) is added to allow for energy sinks other than ridge building (e.g., sliding friction) during shear. In case of convergence, the closing rate must be large enough to satisfy area conservation after ridging, so we take:

$$|\dot{\epsilon}|\alpha_d(\theta) = \max(|\dot{\epsilon}|\alpha_d(\theta), -\nabla \cdot \mathbf{u}|^{trp}) \quad \text{if } \nabla \cdot \mathbf{u} < 0. \quad (5.5)$$

The **opening rate** is obtained by taking the difference:

$$|\dot{\epsilon}|\alpha_o = |\dot{\epsilon}|\alpha_d - \nabla \cdot \mathbf{u}|^{trp} \quad (5.6)$$

### 5.1.2 The two deformation modes: ridging and rafting

The deformation mode is separated into ridging  $w^{ri}$  and rafting  $w^{ra}$  modes:

$$w^d(h, g) = w^{ri}(g, h) + w^{ra}(g, h). \quad (5.7)$$

**Rafting** is the piling of two ice sheets on top of each other. Rafting doubles the participating ice thickness and is a volume-conserving process. Babko et al. (2002) concluded that rafting plays a significant role during initial ice growth in fall, therefore we included it into the model.

**Ridging** is the piling of a series of broken ice blocks into pressure ridges. Ridging redistributes participating ice on a various range of thicknesses. Ridging does not conserve ice volume, as pressure ridges are porous. Therefore, the volume of ridged ice is larger than the volume of new ice being ridged. In the model, newly ridged ice has a prescribed porosity  $p = 30\%$  (*ridge\_por* in *namelist\_ice*), following observations (Leppäranta et al., 1995; Høyland, 2002). The importance of ridging is now since the early works of (Thorndike et al., 1975).

The deformation modes are formulated using **participation** and **transfer** functions with specific contributions from ridging and rafting:

$$w_d(h, g) = -[b^{ra}(h) + b^{ri}(h)]g(h) + n^{ra}(h) + n^{ri}(h). \quad (5.8)$$

$b^{ra}(h)$  and  $b^{ri}(h)$  are the rafting and ridging participation functions. They determine which regions of the ice thickness space participate in the redistribution.  $n^{ra}(h)$  and  $n^{ri}(h)$ , called transfer functions, specify how thin, deformation ice is redistributed onto thick, deformed ice. Participation and transfer functions are normalized in order to conserve area.

### 5.1.3 Participation functions

We assume that the participation of ice in redistribution does not depend upon whether the deformation process is rafting or ridging. Therefore, the participation functions can be written as follows:

$$b^{ra}(h) = \beta(h)b(h), \quad (5.9)$$

$$b^{ri}(h) = [1 - \beta(h)]b(h), \quad (5.10)$$

where  $b(h)$  is an exponential weighting function with an e-folding scale  $a^*$  (Lipscomb et al., 2007) (*astar* in *namelist\_ice*) which preferentially apportions the thinnest available ice to ice deformation:

$$b(h) = \frac{\exp[-G(h)/a^*]}{a^*[1 - \exp(-1/a^*)]}, \quad (5.11)$$

It is numerically more stable than the original version of Thorndike et al. (1975). This scheme is still present in the code and can be activated using *partfun\_swi* from *namelist\_ice*, with the associated parameter *Gstar*.

$\beta(h)$  partitions deformation ice between rafted and ridged ice.  $\beta(h)$  is formulated following Haapala (2000), using the Parmeter (1975) law, which states that, under a critical participating ice thickness  $h_P$ , ice rafts, otherwise it ridges:

$$\beta(h) = \frac{\tanh[-C_{ra}(h - h_P)] + 1}{2}, \quad (5.12)$$

where  $C_{ra} = 5 \text{ m}^{-1}$  (*Craft* in *namelist\_ice*) and  $h_P = 0.75 \text{ m}$  (*hparameter* in *namelist\_ice*) (Haapala, 2000; Babko et al., 2002). The *tanh* function is used to smooth the transition between ridging and rafting. If *namelist* parameter *raftswi* is set to 0, ice only ridges and does not raft.

#### 5.1.4 Transfer functions

The rafting transfer function assumes a doubling of ice thickness :

$$n^{ra}(h) = \frac{1}{2} \int_0^\infty \delta(h - 2h')b(h')g(h')dh, \quad (5.13)$$

where  $\delta$  is the Dirac delta function.

The ridging transfer function is :

$$n^{ri}(h) = \int_0^\infty \gamma(h', h)(1 + p)b(h')g(h')dh. \quad (5.14)$$

The redistributor  $\gamma(h', h)$  specifies how area of thickness  $h'$  is redistributed on area of thickness  $h$ . We follow (Hibler, 1980) who constructed a rule, based on observations, that forces all ice participating in ridging with thickness  $h'$  to be linearly distributed between ice that is between  $2h'$  and  $2\sqrt{H^*h'}$  thick, where  $H^* = 100 \text{ m}$  (*Hstar* in *namelist\_ice*). This in turn determines how to construct the ice volume redistribution function  $\Psi^v$ . Volumes equal to participating area times thickness are removed from thin ice. They are redistributed following Hibler's rule. The factor  $(1 + p)$  accounts for initial ridge porosity  $p$  (*ridge\_por* in *namelist\_ice*, defined as the fractional volume of seawater initially included into ridges. In many previous models, the initial ridge porosity has been assumed to be 0, which is not the case in

reality since newly formed ridges are porous, as indicated by in-situ observations (Leppäranta et al., 1995; Høyland, 2002). In other words, SI<sup>3</sup> creates a higher volume of ridged ice with the same participating ice.

For the numerical computation of the integrals, we have to compute several temporary values:

- The thickness of rafted ice  $h_l^{ra} = 2h_l^i$
- The mean thickness of ridged ice  $h_l^{ri,mean} = \max(\sqrt{H^*h_l^i}, h_l^i \cdot 1.1)$
- The minimum thickness of ridged ice  $h_l^{ri,min} = \min[2 * h_l^i, 0.5 \cdot (h_l^{ri,mean} + h_l^i)]$
- The maximum thickness of ridged ice  $h_l^{ri,max} = 2h_l^{ri,mean} - h_l^{ri,min}$
- The mean rate of thickening of ridged ice  $k_l^{ri} = h_l^{ri,mean} / h_l^i$

### 5.1.5 Ridging shift

The numerical computation of the impact of mechanical redistribution on ice concentration involves:

- A normalization factor that ensures volume conservation (*aksum*)
- The removal of ice participating in deformation (including the closing of open water)
- The addition of deformed ice

For ice concentrations, the numerical procedure reads:

$$\Delta g_l^i = C^{net} \Delta t \left[ - (b_l^{ri} + b_l^{ra}) + \sum_{l_2=1}^L \left( f_{l,l_2}^{ra} \frac{b_{l_2}^{ra}}{k^{ra}} + f_{l,l_2}^{ri} \frac{b_{l_2}^{ri}}{k_{l_2}^{ri}} \right) \right] \quad (5.15)$$

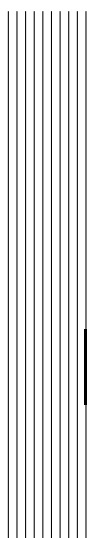
- $C^{net}$  is the normalized closing rate ( $|\dot{\epsilon}| \alpha^d / aksum$ )
- $b_l^{ri}$  and  $b_l^{ra}$  are the area participating into redistribution for category  $l$
- $f_{l,l_2}^{ra}$  and  $f_{l,l_2}^{ri}$  are the fractions of are of category  $l$  being redistributed into category  $l_2$
- $k^{ra}$  is the rate of thickening of rafted ice (=2)

Because of the nonlinearities involved in the integrals, the ridging procedure has to be iterated until  $A^* = A^{ow} + \sum_{l=1}^L g_l^i = 1$ .

### 5.1.6 Mechanical redistribution for other global ice variables

The other global ice state variables redistribution functions  $\Psi^X$  are computed based on  $\Psi^g$  for the ice age content and on  $\Psi^{v^i}$  for the remainder (ice enthalpy and salt content, snow volume and enthalpy). The general principles behind this derivation are described in Appendix A of [Bitz et al. \(2001\)](#). A fraction  $f_s = 0.5$  (*fsnowrdg* and *fsnowrft* in *namelist\_ice*) of the snow volume and enthalpy is assumed to be lost during ridging and rafting and transferred to the ocean. The contribution of the seawater trapped into the porous ridges is included in the computation of the redistribution of ice enthalpy and salt content (i.e.,  $\Psi^{e^i}$  and  $\Psi^{M^s}$ ). During this computation, seawater is supposed to be in thermal equilibrium with the surrounding ice blocks. Ridged ice desalination induces an implicit decrease in internal brine volume, and heat supply to the ocean, which accounts for ridge consolidation as described by [Høyland \(2002\)](#). The inclusion of seawater in ridges does not imply any net change in ocean salinity. The energy used to cool down the seawater trapped in porous ridges until the seawater freezing point is rejected into the ocean.





## 6 Ice thermodynamics

### Contents

---

<b>6.1</b>	<b>Overarching aspects and practical features</b>	<b>44</b>
6.1.1	From / to temperature and enthalpy	46
6.1.2	Control corrections	46
<b>6.2</b>	<b>Approximate energy budget of the first-ocean level</b>	<b>46</b>
<b>6.3</b>	<b>Lateral thermodynamics</b>	<b>47</b>
6.3.1	Ice growth in open water	47
6.3.2	Lateral melting	48
<b>6.4</b>	<b>Vertical thermodynamics</b>	<b>50</b>
6.4.1	Thermal diffusion (temperature calculation)	50
6.4.2	Radiation attenuation and absorption	52
6.4.3	Vertical accretion and ablation	52
6.4.4	Remapping	54
<b>6.5</b>	<b>Transport in thickness space</b>	<b>55</b>
<b>6.6</b>	<b>Melt ponds</b>	<b>57</b>
<b>6.7</b>	<b>Ice salinity</b>	<b>58</b>
<b>6.8</b>	<b>Single-category use</b>	<b>59</b>
<b>6.9</b>	<b>Ice age</b>	<b>60</b>

---

In the world of sea ice modelling, *thermodynamics* refer to the processes that induce a net increase or decrease of sea ice mass. The term is more general than it seems and also encompasses optical (albedo) and fluid transfer (brine drainage, ponds) processes. Following historical developments, sea ice thermodynamics in SI3 are split into vertical thermodynamics and lateral processes. They also include a treatment of snow, melt ponds and ice salinity. Most features can be activated

using logical namelist parameters. Thermodynamic calculations require heat and mass fluxes from the atmosphere and the ocean, affect all model variables except drift velocity, and produce energy and mass fluxes to the atmosphere and the ocean in return. Sea ice albedo, sea ice-ocean freshwater fluxes, and sea ice thickness, key targets of contemporary climate, ocean and operational sea ice model applications, are the key outcomes of sea ice thermodynamic calculations.

## 6.1 Overarching aspects and practical features

```

!-----
&nampar          !   Generic parameters
!-----
  jpl             = 5           !   number of ice categories
  nlay_i          = 2           !   number of ice layers
  nlay_s          = 2           !   number of snow layers
  ln_virtual_itd = .false.     !   virtual ITD mono-category
    ↪ parameterization (jpl=1 only)
                                !   i.e. enhanced thermal
                                ↪ conductivity & virtual thin
                                ↪ ice melting
  ln_icedyn       = .true.     !   ice dynamics (T) or not (F)
  ln_icethd       = .true.     !   ice thermo (T) or not (F)
  rn_amax_n       = 0.997     !   maximum tolerated ice
    ↪ concentration NH
  rn_amax_s       = 0.997     !   maximum tolerated ice
    ↪ concentration SH

```

**Listing 3:** SI3 namelist, generic section

```

!-----
&namthd          !   Ice thermodynamics
!-----
  ln_icedH        = .true.     !   activate ice thickness change
    ↪ from growing/melting (T) or not (F)
  ln_icedA        = .true.     !   activate lateral melting param.
    ↪ (T) or not (F)
  ln_icedO        = .true.     !   activate ice growth in open-water
    ↪ (T) or not (F)
  ln_icedS        = .true.     !   activate brine drainage (T) or
    ↪ not (F)
  !
  ln_leadhrefx   = .true.     !   heat in the leads is used to melt
    ↪ sea-ice before warming the ocean

```

**Listing 4:** SI3 namelist, section ice thermodynamics

As classically done, sea ice thermodynamics are treated as *column* processes. This includes processes that are not all purely vertical, but that can be handled without considering x- and y- dependencies. They include *vertical* processes (heat diffusion, growth and melt, desalination, ...), and so-called *lateral* processes related

to exchanges with open water. Other calculation steps are more formal or numerical, such as the conversion from extensive to intensive variables, or the transport in thickness space, needed to redistribute ice into categories.

```

! === icesbc_flux.F90 === !
CALL ice_alb                ! --- Surface albedo      --- !
[surface fluxes (various options)]
CALL ice_flux_other         ! --- Bottom fluxes and lead energy budget --- !

! === icethd.F90 === !
[2d-1d swap]
CALL ice_thd_zdf            ! --- Diffusion of heat      --- !
CALL ice_thd_dh             ! --- Growth and melt       --- !
CALL ice_thd_ent            ! --- Ice enthalpy remapping --- !
CALL ice_thd_sal            ! --- Ice salinity          --- !
CALL ice_thd_temp           ! --- Recover temperature from enthalpy --- !
CALL ice_thd_da             ! --- Lateral melting       --- !

[1d-2d swap]
CALL ice_thd_pnd            ! --- Melt ponds            --- !
CALL ice_itd_rem            ! --- Transport ice between thickness categories --- !
CALL ice_thd_do             ! --- Frazil ice growth in leads --- !
[corrections and ice age incrementation]

```

**Figure 6.1:** Schematic sequence of thermodynamic calculations from `icestp.F90`

The sequence of thermodynamic calculations is summarized in Fig. 6.1. Preparatory steps in `ice_stp` include conversion from extensive to intensive variables (`ice_var_glo2eqv`), as well as calculation of thermodynamic forcing (`ice_sbc_flux`). Then, the main thermodynamic routine `ice_thd` is called, where vertical and lateral processes, including melt ponds and salinity calculations are performed.

In order to reduce CPU and memory use, thermodynamic calculations are whenever possible performed only where they are needed in the domain. This is achieved with 2D-1D array conversions, performed in several instances, such as in the beginning of `ice_thd`.

Vertical thermodynamic calculations are repeated for each ice thickness category (total number `jpl`), whereas lateral calculations need to be performed once. Categories imply larger CPU and memory use but are useful physically. Users seeking to reduce CPU and memory burden may use a single category (set `jpl` to 1) and activate (`ln_virtual_itd`), which emulates multi-category physics in a single-category framework (see specific subsection below).

In idealized simulations, users may find useful to disable ice thermodynamics, which is what `ln_icethd` is made for. It removes the call to `ice_thd`, and assumes no air-sea exchanges in ice-covered seas.

### 6.1.1 From / to temperature and enthalpy

Temperature is needed for the diffusion of heat, but is not conservative, whereas enthalpy is conservative but is pointless in the calculation of conductive heat fluxes. Hence conversions from one to the other must be performed at several locations in the code. `ice_var_enthalpy` calculates snow and ice enthalpy from temperature and salinity, whereas `ice_thd_temp` inverts the enthalpy to temperature equation, assuming salinity is fixed, and solves the resulting second-order equation.

### 6.1.2 Control corrections

At the end of thermodynamic calculations, some quality control tests are performed in `ice_cor`. Most of these target elimination of numerical issues associated with very small numbers. Ice thinner than `rn_hmin` is artificially thickened to `rn_hmin`, and associated concentration is reduced in proportion. Salinity must remain in bounds (`rn_simin`, `rnsimax`), and small ice chunks with either concentration, volume or thickness below  $10^{-10}$  are removed in a heat and mass-conserving manner (`ice_var_zapsmall`).

A last but important correction is the ice concentration capping below `rn_amax_n` in the Northern hemisphere (`rn_amax_s` in the South). Equivalent to imposing a minimum lead fraction, this correction compensates for the inability of ice dynamics to maintain the small amount of open water that is observed and provides efficient means to tune sea ice volume (Wang et al., 2010).

## 6.2 Approximate energy budget of the first-ocean level

As part of the sea ice computations in `ice_flx_other`, a heat budget of the uppermost oceanic level is estimated, following ideas developed in Fichefet and Gaspar (1988). This heat budget serves new ice production if negative or bottom melting if positive.

The heat budget of the first ocean level (`q_lead`) is approximated assuming four contributions, namely (i) the absorption of a fraction `frq_m` of solar radiation (computed within ocean light attenuation calculations); (ii) the non-solar heat flux absorbed at the open water surface; (iii) the sensible heat content of precipitation; (iv) the sensible heat loss to the sea ice. This heat budget is approximate as there is no consideration of the entrainment of heat at the base of the first ocean level, or of solar radiation transmitted below the ice. The ocean-to-ice turbulent sensible heat flux (`qsb_ice_bot`) is formulated following (McPhee, 1992):

$$F_w = \rho_0 c_w C_h u^* (SST - T_b), \quad (6.1)$$

where  $\rho_0$  is the reference ocean density,  $c_w$  is the seawater specific heat,  $C_h = 7.5 \times 10^{-3}$  is a heat transfer coefficient, and  $u^* = \sqrt{\tau_{iw}/\rho_0}$  is a friction velocity.



Figure 6.2: Scheme of the estimate of the heat budget of the first ocean level.

There are two additional conditions, first the oceanic heat flux cannot be negative, second,  $F_{w.rdt\_ice}$  cannot exceed the heat content of the first ocean level.

If the open water energy budget is such that the SST would decrease below the freezing point, the excess heat loss ( $zqfr\_neg$ ) is saved for new ice formation. If there is ice in the grid cell and that the  $q\_lead$  is positive, it is directly added to the heat available for bottom melting. This argument follows from [Maykut and McPhee \(1995\)](#), who found that most of solar heat absorbed in the surface waters is converted into ice melting. In practise, this means that the SST can hardly go above freezing as long ice is present. The heat loss used for ice formation, heat gain used to melt ice and the sensible heat given by the ocean to the ice, are all removed from the non-solar heat flux transmitted to the ocean, in `ice_udpate_flux`.

## 6.3 Lateral thermodynamics

### 6.3.1 Ice growth in open water

Ice growth in open water section (`ice_thd_do`) converts negative heat available for freeze-up into a volume of new sea ice and assigns this new ice a thickness, an area, enthalpy, and salt content, and redistributes these into relevant ice categories.

The key input is `qlead_1d`, the available negative heat for freeze up, computed in `ice_flux_other`. Only grid points with negative heat loss are retained in the calculation and 1D arrays are retained accordingly.

```

!-----
&namthd_do      !   Ice growth in open water
!-----
rn_hinew       = 0.1           ! thickness for new ice formation
↳ in open water (m), must be larger than rn_himin
ln_frazil      = .false.      ! Frazil ice parameterization (ice
↳ collection as a function of wind)
rn_maxfraz     = 1.0           ! maximum fraction of frazil ice
↳ collecting at the ice base
rn_vfraz       = 0.417        ! threshold drift speed for
↳ frazil ice collecting at the ice bottom (m/s)
rn_Cfraz       = 5.0           ! squeezing coefficient for
↳ frazil ice collecting at the ice bottom

```

**Listing 5:** SI3 namelist, section ice growth in open water

To convert  $q_{lead\_ld}$  into an ice volume, the enthalpy of the new ice (J/kg) is specified from assumed salinity and temperature for new ice.  $S_{new}$  depends on the representation of salinity ( $nn\_ice\_sal$ , see Section XX), whereas  $T_{new} = T_{fr}(SSS)$ . In summary, the volume of new ice is calculated as:

$$V_{new} = \frac{\rho_i Q_{lead}}{E_i(SSS, T_{fr}) - E_w(SSS, T_{fr})}, \quad (6.2)$$

which assumes that the source water is already at the freezing point.

To assign new ice a fractional area,  $V_{new}$  is divided by new ice thickness, which depends on unresolved small currents and waves and must be imposed. By default ( $ln\_frazil = .false.$ ), new ice thickness  $rn\_hinew$  is set to a constant, typically 0.1 m. If  $ln\_frazil$  is activated, in `ice_thd_frazil` new ice thickness is calculated based on the polynya model of Biggs et al. (2000) as a function of wind speed and sea ice velocity, also referred to as *collection thickness* (i.e. accumulated at the edges of leads and polynyas).

Once new ice area fraction is known, new ice properties can be merged into categories, depending on thickness. By default, new ice area is added to the category its thickness falls into. However, if the new ice area exceeds the available open water area ( $A_{max} - A$ ), the excess ice volume, enthalpy and salt content is added at the ice base into the existing categories, in proportion of their pre-existing area but without changing it. If  $ln\_frazil$  is activated, a fraction of the new ice volume ( $fraz\_frac$ ), is also added at the base of the categories. This fraction is calculated as a hyperbolic tangent function of wind speed (pivotal value  $rn\_vfraz$ , width of the step  $rn\_Cfraz$ ).  $rn\_maxfraz$  sets the maximum fraction of new ice volume that can be accreted at the ice base (1 by default).

### 6.3.2 Lateral melting

Lateral melting (`ice_thd_da`) reduces ice concentration, wherever SST is above freezing, by imposing a lateral melt rate  $w$  function of SST and ice concen-

```

!-----
&namthd_da      !   Ice lateral melting
!-----
rn_beta         =   1.0   !   Coef. beta for lateral melting
rn_dmin        =   8.    !   Minimum floe diameter for lateral melting

```

**Listing 6:** SI3 namelist, section lateral melting

tration (Bitz et al., 2001):

$$\frac{dA}{dt} = w(SST).P(A). \quad (6.3)$$

$w$  is parameterized from a boundary layer parameterization (Josberger and Martin, 1981):  $w = m_1(SST - T_{fr})^{m_2}$ .  $m_1$  and  $m_2$  were tuned to observations of lateral melting in the Greenland Sea in 1984 (Maykut and Perovich, 1987).  $P(A) = A\pi/[0.66.D(A)]$  is the mean floe perimeter per unit area, calculated assuming floes are quasi-circular (Rothrock and Thorndike, 1984) and have a diameter relating to ice concentration following Fram Strait aircraft observations Lüpkes et al. (2012):

$$D = rn\_dmin \left( \frac{A^*}{A^* - A} \right)^{rn\_beta}. \quad (6.4)$$

Area fraction of categories is affected in proportion of pre-existing fractional area. Resulting salt, heat and mass fluxes are calculated a posteriori from the salt, heat and mass content of the molten ice categories. Lateral concentration loss rate for standard parameters is depicted in Fig. 6.3.

$rn\_dmin$  and  $rn\_beta$  control the floe-diameter-concentration relationship, are highly variable from one region to another and can be used as tuning parameters for the strength of lateral melting and how it depends on concentration. Higher  $rn\_dmin$  effectively reduces lateral melt rate, whereas increasing  $rn\_beta$  moves the lateral melt rate maximum towards low concentration values and reduces melt rate.

## 6.4 Vertical thermodynamics

### 6.4.1 Thermal diffusion (temperature calculation)

$icethd\_zdf$  manages internal temperature and (optionally) surface temperature calculations, by resolving the coupled surface energy balance and heat diffusion equations:

$$\begin{cases} Q^{sr} + Q^{ns}(T_{su}) &= Q^c(T_{su}, T), \\ \rho c_p(S, T) \frac{\partial T}{\partial t} &= \frac{\partial}{\partial z} \left[ k(S, T) \frac{\partial T}{\partial z} \right] + R(z), \end{cases} \quad (6.5)$$

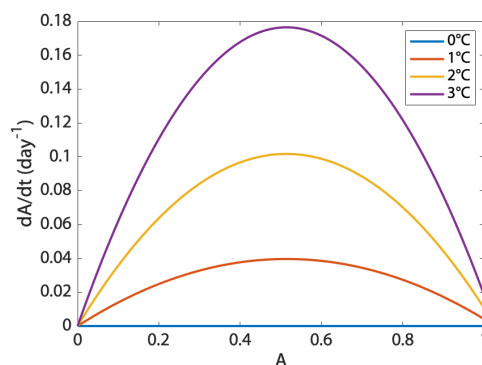


**Figure 6.3:** Lateral melt rate as a function of ice concentration and SST departure from the freezing point for reference parameters ( $rn\_beta = 1$ ,  $rn\_dmin = 8$  m).

with  $T = T_{fr}(SSS)$  as a boundary condition at the ice base.  $Q^{sr}$  is net solar flux, including the albedo contribution,  $Q^{ns}$  is net non-solar flux,  $Q^c$  is inner conduction flux;  $\rho$  is density (constant),  $c_p$  is specific heat capacity,  $k$  is thermal conductivity, and  $R$  is absorption of solar energy ( $J/m^3/s$ ).

The input fields for temperature calculations include the incident net solar heat flux at the ice surface ( $qsr\_ice$ ), the solar flux transmitted below the surface layer ( $qtr\_ice\_top$ ), and the net non-solar heat flux ( $qns\_ice$ ), including the longwave down, latent and sensible heat contributions. The iterative procedure implies the need for the non-solar heat flux derivative with respect to temperature ( $dqns\_ice$ ).  $qtr\_ice\_top$ , the solar heat transmitted below the surface layer, must also be provided. Outputs are the vertical snow-ice temperature profile (and associated enthalpy), and, optionally, the surface temperature.

Two formulations for surface energy flux handling are implemented. In the *standard* formulation ( $ln\_cndflx=.false.$ ),  $Q^{sr}$ ,  $Q^{ns}$  are imposed and  $T_{su}$  is calculated from surface energy balance (Bitz and Lipscomb, 1999). In the *conduction* formulation ( $ln\_cndflx=.true.$ ), the top conductive flux is imposed as an upper boundary condition in the heat equation, the surface energy balance is bypassed, and the surface temperature is diagnosed for outputs only (West et al., 2016).  $ln\_cndemulate$  is there for testing the conduction flux formulation. With that option on, thermal diffusion is called twice. In the first call, the conduction flux is diagnosed from the *standard* formulation, and in the second call, the calculated top  $Q^c$  is used as surface forcing for the *conduction* formulation.

A single algorithm (Bitz and Lipscomb, 1999) is currently implemented under the  $ln\_zdf\_BL99$  flag to solve the surface energy balance and heat diffusion

```

!-----
&namthd_zdf      !   Ice heat diffusion
!-----
ln_zdf_BL99      = .true.    ! Heat diffusion numerical scheme of Bitz
  ↳ and Lipscomb (1999)
ln_cndi_U64      = .false.   ! Sea ice thermal conductivity: k = k0 +
  ↳ beta.S/T (Untersteiner, 1964)
ln_cndi_P07      = .true.    ! Sea ice thermal conductivity: k = k0 +
  ↳ beta1.S/T - beta2.T (Pringle et al., 2007)
rn_cnd_s         = 0.31     ! Snow thermal conductivity (0.31 W/m/K,
  ↳ Maykut and Untersteiner, 1971)
                                     ! Obs: 0.1-0.5 (Lecomte et al, JAMES
                                     ↳ 2013)
rn_kappa_i       = 1.0      ! Attenuation coefficient in sea ice
  ↳ [1/m]
rn_kappa_s       = 10.0     ! nn_qtrice = 0: Attenuation coefficient
  ↳ in snow [1/m]
rn_kappa_smlt    = 7.0      ! nn_qtrice = 1: Attenuation coefficient
  ↳ in melting snow [1/m]
rn_kappa_sdry    = 10.0     ! radiation attenuation coefficient
  ↳ in dry snow [1/m]
ln_zdf_chkcvg    = .false.   ! Check convergence of heat diffusion
  ↳ scheme (outputs: tice_cvgr, tice_cvgstp)

```

Listing 7: SI3 namelist, section vertical thermodynamics

equations:

$$\begin{cases}
(\kappa_{su} + \partial_{T_{su}} Q^{ns}) T_{su}^{n+1} + \kappa_{su} T_1^{n+1} = \partial_{T_{su}} Q^{ns} \cdot T_{su}^* - Q_{net}^*, \\
\dots \\
T_{k-1}^{n+1} [-\eta_k \kappa_{k-1}] + T_k^{n+1} [1 + \eta_k (\kappa_{k-1} + \kappa_k)] + T_{k+1}^{n+1} [-\eta_k \kappa_{k+1}] = T_k^n + \eta_k R_k. \\
\dots
\end{cases} \quad (6.6)$$

The temporal discretization is first-order and implicit. Because  $Q^{ns}$ ,  $c_p$  and  $k$  are non-linear in  $T$ , the system must be iterated. \* refers to previous sub-iterate. Also, the temperature derivative of the non-solar flux  $\partial_{T_{su}} Q^{ns}$  must be provided.

The vertical discretization uses a vertical z-coordinate grid and second-order-in-space discrete expressions for the conductive heat fluxes. The number of snow and ice layers (`nlay_i`, `nlay_s`) is fixed and all ice and snow layers have equal thickness.  $\kappa_k$  factors are layer conductivities divided by layer thickness, and  $\eta_k = \rho \Delta t \Delta h_k / c_{p,k}$  are written so as to preserve energy conservation (Bitz and Lipscomb, 1999).

Equations 6.6 form a tridiagonal system that is solved at each sub-iteration using the Thomas algorithm. The whole algorithm is not exactly conservative – errors are on the order of  $10^{-4}$  W/m<sup>2</sup>. The conservation error is diagnosed and added to the heat flux transmitted to the ocean (`hfx_err_dif`). Iterations stop once the maximum temperature change in a given sub-iteration is smaller than  $10^{-4}$  °C. The temperature error at convergence and number of iterations to convergence can be diagnosed if the `ln_zdf_chkcvg` flag is activated.

As written, the equations 6.6 simplify the actual code calculations. Surface and bottom layer equations take a close but different form because of boundary conditions. Also, the number of equations in the tridiagonal system, and its different terms change with the presence/absence of snow. The tridiagonal system also changes whether the surface is melting ( $T_{su} = 0$ ) or not. If snow depth is non-zero, extra equations for each snow layer temperature are considered. If the surface energy balance is such that the surface temperature is above zero, the latter is set to zero, and the tridiagonal system is amputated of the surface equation in the next sub-iteration. The tridiagonal system also changes in the case the *conductive* formulation is used.

Because of substantial uncertainties in thermal conductivity of sea ice, there are several namelist options. There are two formulations for sea ice thermal conductivity: `ln_cndi_U64` triggers the classical expression of [Untersteiner \(1964\)](#), and `ln_cndi_P07` triggers the formulation of [Pringle et al. \(2007\)](#). The thermal conductivity of snow is assumed constant and can be directly set up from the namelist (`rn_cnd_s`).

#### 6.4.2 Radiation attenuation and absorption

Two formulations are available for shortwave radiation absorption and transmission through snow and sea ice. Both formulations assume exponential attenuation for downwelling transmitted radiation  $Q_{tr}$  at depth  $z$ :

$$Q_{tr} = qtr\_ice\_top \cdot \exp(-\kappa z), \quad (6.7)$$

where  $qtr\_ice\_top = i_o \cdot qsr\_ice$  is the solar flux transmitted below the ice surface, with  $i_o$  is surface transmission parameter and  $\kappa$  the vertical attenuation coefficient. The simplest formulation (`nn_qtr_ice=0`) is from [Fichefet and Morales Maqueda \(1997\)](#) and `q` assumes no transmission of radiation through snow and specifies  $i_o$  as a function of cloud fraction ([Grenfell and Maykut, 1977](#)). In the second formulation ([Lebrun, 2019](#)), which specificity is that it was carefully tuned to Arctic transmittance observations,  $i_o$  is non-zero even when snow is present and has snow attenuation coefficients depending on surface wetness. This scheme presently generates issues with surface melting, probably because of the lack of internal snow melting and is not yet recommended.

Radiative transfer calculations are repeated for snow-covered and snow-free parts of the sea ice column in each ice thickness category. Snow area fraction treatment depends on `nn_snowfra`. If zero, snow fraction is 1. Two empirical calculation methods are provided: an exponential formulation (`nn_snowfra = 1`,  $A_s = 1 - \exp(-0.2\rho_s h_s)$ ) and a logistic one (`nn_snowfra = 2`,  $A_s = h_s / (0.02 + h_s)$ ).

Radiative transfer calculations in SI3 are independent of temperature and are therefore performed before the temperature iterative procedure, at the beginning of `icethd_zdf_b199`. Transmitted fluxes at the base of each ice and snow layer are first calculated, then the absorbed radiation in each layer  $R_k$  is calculated, as

bottom minus top transmitted flux divided by thickness. The transmitted radiation flux at the based sea ice (`qtr_ice_bot`) is sent to the ocean.

### 6.4.3 Vertical accretion and ablation

The next step (processed in `ice_thd_dh`) is to add and/or remove snow and ice mass due to vertical processes. For congelation growth and melt, the change in thickness  $\Delta h_x$  for medium  $x$  (snow or ice) and process  $y$  stems from an energy excess or loss  $Q_y$ , and is calculated as follows:

$$\Delta h_x \Big|_y = \frac{Q_y}{\rho_x E_x(S_y, T_y)}, \quad (6.8)$$

where  $\rho$  is density,  $E$  is specific enthalpy,  $S$  and  $T$  are salinity and temperature. For snow fall and snow ice formation, the mass flux must be specified.

Generally, the required fields to calculate vertical growth and melt include the energy budget components at the air-ice and ice-ocean interfaces ( $\text{W/m}^2$ ); and the external mass (and associated sensible heat) fluxes. The air-ice energy budget components are: the non-solar and net solar surface fluxes (`qns_ice`, `qsr_ice`), the inner heat conduction flux `qcn_ice_top`, and the solar flux transmitted below the surface (`qtr_ice_top`). The ice-ocean energy budget components are the inner heat conduction flux `qcn_ice_bot`, the sensible ocean-to-ice heat flux (`qsb_ice_bot`), the upper ocean level heat budget excess (`fhld`), and the solar radiation flux transmitted below sea ice (`qtr_ice_bot`). Of the latter, only the fraction `frq_m_1d` absorbed in the first ocean level is considered. `frq_m_1d` is calculated in the ocean component. From all these, the heat available for melting is diagnosed at air-ice and ice-ocean interfaces. External mass fluxes and associated sensible heat are also needed, namely snowfall rate (`sprecip`,  $\text{kg/m}^2/\text{s}$ ), the enthalpy of falling snow (`qprec_ice`,  $\text{J/m}^3$ ), as well as the evaporative mass flux (`evap_ice`,  $\text{kg/m}^2/\text{s}$ ).

#### Snow mass sources and sinks

The considered sources and sinks of snow mass are snowfall, surface and internal melting, sublimation and snow-ice formation.

A fraction  $(1 - A)^{\text{rn\_snwblow}}$  of **snowfall** goes into open water due to blowing snow. With the blowing snow parameter `rn_snwblow=1`, blowing snow effect is off, and the fraction of snow falling in open water is  $(1 - A)$  (the open water fraction). With `rn_snwblow < 1`, a larger snow fraction falls into ocean and so less snow falls on sea ice. Snow falling onto sea ice is converted into snow accumulation assuming constant snow density and increases snow depth on sea ice. Corresponding fractions of the sensible heat of solid precipitation are routed to the ocean surface and to a temporary new snow layer at the snow surface. In practice, `rn_snwblow` is useful to tune snow depth. Liquid precipitation and its heat content integrally goes into open water.

Snow melts at the surface when  $T_{su} = 0^\circ\text{C}$  and  $Q_{melt} > 0$ . **Surface melting** is diagnosed by removing a layer of thickness  $\Delta h_s = Q_{melt}/(\rho_s E_s)$ , layer by layer, from top to bottom, until  $Q_{melt}$  is exhausted. In the case some of this heat remains after melting all snow, the remainder is used for melting sea ice. **Internal melting** of snow occurs when the temperature one of the snow layers exceeds  $0^\circ\text{C}$ , either because of the deposition of heat by solar radiation into the snow, or to spurious behaviour of the thermal diffusion calculation algorithm. In either case, snow layers with temperature above zero are removed, in a heat/water conserving manner.

**Sublimation** converts the evaporation mass flux `evap_ice` into a snow loss assuming constant density. The energy cost of sublimation is included in the latent heat flux and needs not being accounted for. Evaporation removes snow mass, and is handled layer by layer. Deposition of snow if any should be routed through the solid precipitation mass flux.

Snow is also removed if sea ice melts entirely, and through the formation of snow-ice (see next section).

### Sea ice mass balance

The considered sources and sinks of ice mass are basal growth, snow-ice formation, surface melt and basal melt.

**Melting and sublimation** of sea ice proceed similarly as for snow. Ice enthalpy instead of snow enthalpy is used. Bottom melting proceeds upwards from bottom layer, instead of downwards for surface melting.

**Basal growth** converts basal energy budget (`zf_tt`), if negative, into a layer of new ice. As the new ice salinity depends on growth rate, the calculation must be iterated (this feature will soon become obsolete).

*Snow ice.* When snow is deep enough to depress the snow-ice interface below the sea level, seawater infiltrates and refreezes into the snow, creating a new layer of sea ice on top of pre-existing ice, with thickness [Fichefet and Morales Maqueda \(1997\)](#):

$$\Delta h = \frac{\rho_s h^s - (\rho_w - \rho_i) h^i}{\rho_s + \rho_w - \rho_i}, \quad (6.9)$$

where  $\rho_w$  and  $\rho_s$  are the reference densities of seawater and snow, respectively. The enthalpy of the new ice is a weighted mean of those of snow and melt water ([Jutras et al., 2016](#)). The increment in snow depth is the opposite of the increment in ice thickness.

### Ice-ocean exchanges

Total melt water is cumulated in the water flux to the ocean, for each contributing process, and for each category. Any water flux goes along with a sensible heat flux. Sublimation mass and the associated sensible heat flux can be sent back to the atmosphere if the atmospheric component allows it.

### 6.4.4 Remapping

$nlay\_s$  layers of snow and  $nlay\_i$  layers of sea ice, of equal thickness, are assumed. Hence, after ice growth and melt, temperatures at the mid-point have to be recomputed. This is done by redistributing the enthalpy per unit area  $Q^x = q^x \Delta h^x$  ( $J/m^2$ ) on the new grid, in an energy-conserving manner. This *vertical remapping* is illustrated for one particular case in Fig. 6.4, and calculated in `ice_thd_ent`.

The procedure implies to properly reference the position layers and their enthalpy at the end of growth and melt processes, and to redistribute them, in a linear fashion, on the new grid. In other words, the  $Q^x$  are linearly redistributed from the old to the new grid:

$$Q_k = \sum_{k'} w_{k,k'} Q_{k'}^{old}. \quad (6.10)$$

The weight factors  $w_{k,k'}$  give the contribution of each *old* layer to the *new* layers. Finally, the new enthalpies  $Q^k$  are converted into specific enthalpies  $q^x$  and then, into temperatures  $T^k$ .

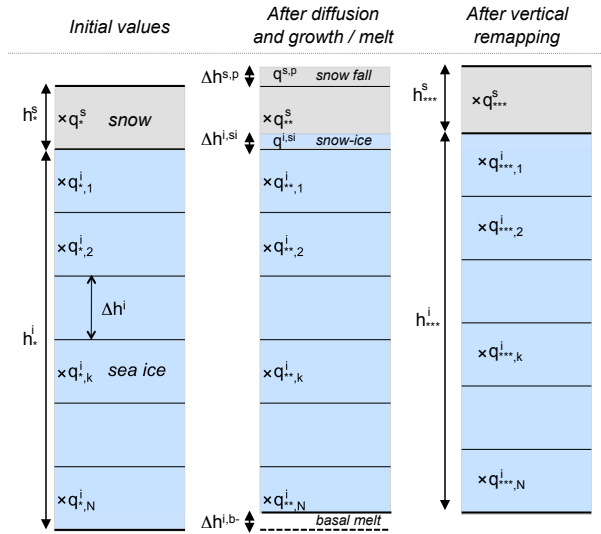


**Figure 6.4:** An illustration of the vertical enthalpy remapping procedure in a case for which snow falls, snow ice forms and ice melts at the base.

## 6.5 Transport in thickness space

As ice categories have fixed boundaries in thickness space, changes in ice thickness due to vertical thermodynamics imply that some ice must be transferred between

neighboring categories. This is what is referred to as transport in thickness space and is handled in `ice_itd_rem`.

The need for transporting ice in thickness space following thermodynamics stems from the use of the thickness distribution framework and can be identified from the conservation of area due in presence of vertical growth and melt processes only (Thorndike et al., 1975):

$$\frac{\partial g}{\partial t} = -\frac{\partial(fg)}{\partial h}. \quad (6.11)$$

As noted by Lipscomb (2001), this equation is analogous to a one-dimensional continuity equation in which  $g$  the ice thickness distribution would be equivalent to density and  $f = dh/dt$  [m/s], the rate of change of ice thickness, would correspond to a velocity in thickness space.

The main input field are all extensive variables after all thermodynamic processes, and thicknesses before thermodynamics, which are required to compute thermodynamic velocities, are deduced by comparing thickness after and before vertical growth and melt.

The numerical method used is that of Lipscomb (2001), from which the SI3 code for this part has readily been derived. This is a second-order, semi-lagrangian scheme, which is less diffusive and converges faster than other ones. The scheme is valid as long as the velocities in thickness space are not too large. In this case, following (Bitz et al., 2001), we use a representation in terms of delta functions (`ice_itd_reb`).

Let us consider the thickness distribution discretization presented in Section 3.1. The ice categories are considered as lagrangian cells moving in thickness space. The scheme is based on three steps: (i) displacement of the category boundaries; (ii) approximation of the thickness distribution on the displaced categories; (iii) restoration of the original boundaries.

At time  $n$ , each category  $l$  is covered by an ice area  $g_{l,n}^i$  of thickness  $h_{l,n}^i$ . Using the thermodynamic component described in the previous section, the new thicknesses  $h_{l,n+1}^i$  are computed. The ice growth rate in category  $l$  is  $f_l = (h_{l,n+1}^i - h_{l,n}^i)/\Delta t$ . The ice growth rate at the category boundaries  $F_l$  is linearly interpolated:

$$F_l = f_l + \frac{f_{l+1} - f_l}{h_{l+1}^i - h_l^i} (H_l - h_l^i). \quad (6.12)$$

If both adjacent categories have  $g_m^i = 0$ , then  $F^l$  is chosen to be zero. If one of the adjacent categories has no ice, then we assign to  $F_l$  the value of the non zero category. At time  $n + 1$ , the category boundaries are:  $H_l^* = H_l + F_l \Delta t$ . The area in the displaced categories is conserved, such that  $g_{l,n+1}^{*i} = g_{l,n}^i$ , while the volume is  $v_{l,n+1}^{*i} = g_{l,n}^{*i} h_{l,n+1}^i$ . To work properly,  $H_{l-1} < H_l^* < H_{l+1}$  must be verified. Let us replace  $H_{l-1}^* = H_L$  and  $H_l = H_R$ .

To compute how much ice is transferred between categories, we must build an

approximation for  $g(h)$  in each displaced category, verifying:

$$g_{l,n+1}^{*i} = \int_{H_L}^{H_R} g(h)dh, \quad (6.13)$$

$$v_{l,n+1}^{*i} = \int_{H_L}^{H_R} g(h)h dh. \quad (6.14)$$

A linear polynomial approximation is suitable:  $g(\eta) = g_0 + g_1\eta$ , where  $\eta = h - H_L$ . This function, computed by **lim\_itd\_fitline**, takes 3 forms, whether  $h_{l,m+1}^i$  is in the first, the second or the third part of the interval  $[H_L, H_R]$ .

Once we constructed the displaced thickness distribution, we can remap the thickness distribution to the original boundaries. To do this, in the case of a transfer from  $l$  to  $l + 1$  categories, we have to integrate  $g(h)$  between  $H_l$  and  $H_l^*$ :

$$\Delta g_l^i = \int_{H_l}^{H_l^*} g(h)dh, \quad (6.15)$$

$$\Delta v_l^i = \int_{H_l}^{H_l^*} hg(h)dh. \quad (6.16)$$

The change in other state variables due to transport in thickness space is  $X\Delta v_l^i/v_l^i$  if the variable follows ice volume and  $X\Delta g_l^i/g_l^i$  if the variable follows ice concentration. This is done by routine **lim\_itd\_shiftice**.

## 6.6 Melt ponds

Since the 3.6 release, several melt pond schemes have been included in SI3. They can be activated via `ln_pnd`. There are three formulations: *constant*, *level-ice* and *topographic* melt ponds. Melt ponds are characterized by a volume and area of melt water per unit grid cell area (`v_ip` and `a_ip`). Each of the three schemes does something specific to these two variables, from simple prescription to a more complex calculation based on considerations on surface meltwater runoff, accumulation and drainage [Flocco and Feltham \(2007\)](#).

Essentially, melt ponds are included in order to represent their effect on surface albedo, which can be activated or not (`ln_pnd_alb`). They also hold some freshwater, and release it to the ocean when they decay (`wfx_pnd`).

The CST (`ln_pnd_CST`) scheme assumes constant fraction of the ice-covered grid cell (`rn_apnd`) to be covered by ponds of constant thickness (`rn_hpnd`).

The LEV scheme (activable through `ln_pnd_LEV`) is a mixture of different schemes described in the literature. Each category has its own pond fraction and volume. Pond volume increases / decreases via melt water, overflow, lid melting and loses area through drainage. `rn_pnd_flush` describes the efficiency of flushing.

The TOPO scheme is that of [Flocco and Feltham \(2007\)](#) and calculates . The key difference with the LEV scheme is mostly that pond water is redistributed

```

!-----
&namthd_pnd      !  Melt ponds
!-----
ln_pnd           = .true.           !  activate melt ponds or not
ln_pnd_TOPO     = .false.          !  topographic melt ponds
ln_pnd_LEV      = .true.           !  level ice melt ponds
rn_apnd_min     = 0.15             !  minimum meltwater fraction
  ↪ contributing to pond growth (TOPO and LEV)
rn_apnd_max     = 0.85             !  maximum meltwater fraction
  ↪ contributing to pond growth (TOPO and LEV)
rn_pnd_flush    = 0.1             !  pond flushing efficiency
  ↪ (tuning parameter) (LEV)
ln_pnd_CST      = .false.          !  constant melt ponds
rn_apnd         = 0.2             !  prescribed pond fraction, at
  ↪ Tsu=0 degC
rn_hpnd         = 0.05            !  prescribed pond depth, at
  ↪ Tsu=0 degC
ln_pnd_lids     = .true.           !  frozen lids on top of the ponds
  ↪ (only for ln_pnd_LEV)
ln_pnd_alb      = .true.           !  effect of melt ponds on ice
  ↪ albedo

```

**Listing 8:** SI3 namelist, section melt ponds

among categories from assumptions on the connection between topography and the ice thickness distribution.

Ponds can refreeze, in which case a lid can appear (activabel through `ln_pnd_lids`), masking the effect of ponds on surface albedo.

## 6.7 Ice salinity

SI3 has three options for ice salinity: constant salinity (`nn_icesal=1`), varying in space but not in time (3) and varying in space and time (2).

In the case of vertically varying salinity (3), ice salinity equals `rn_icesal`. In the third case, the ice salinity is prescribed using a typical multi-year ice profile, that is there for historical reasons. This option is basically obsolete and will be removed.

In the third case, the bulk ice salinity follows a prognostic equation, introduced by [Vancoppenolle et al. \(2009a\)](#):

$$\Delta \bar{S}^i = (S^b - \bar{S}^i) \frac{\Delta h^{i,b+}}{h^i} + (S^{si} - \bar{S}^i) \frac{\Delta h^{i,si}}{h^i} - \left( \frac{\bar{S}^i - S^G}{T^G} \right) I^G \Delta t - \left( \frac{\bar{S}^i - S^F}{T^F} \right) I^F \Delta t. \quad (6.17)$$

The terms on the right-hand side refer to basal ice formation, snow ice formation, gravity drainage and flushing, respectively. Gravity drainage and flushing are represented as restoring processes, each of which is characterized by a restoring time scale (`rn_time_gd`, `rn_time_fl`) and salinity (`rn_sal_gd`, `rn_sal_fl`).

```

!-----
&namthd_sal      !   Ice salinity
!-----
  nn_icesal      =   2           !   ice salinity option
                                !   1: constant ice salinity
                                ↪   (S=nn_icesal)
                                !   2: varying salinity
                                ↪   parameterization S(z,t)
                                !   3: prescribed salinity profile
                                ↪   S(z) (Schwarzacher 1959)
  rn_icesal      =   4.         !   (nn_icesal=1) ice salinity
                                ↪   (g/kg)
  rn_sal_gd      =   5.         !   (nn_icesal=2) restoring ice
                                ↪   salinity, gravity drainage (g/kg)
  rn_time_gd     =   1.73e+6    !   (nn_icesal=2) restoring time
                                ↪   scale, gravity drainage (s)
  rn_sal_fl      =   2.         !   (nn_icesal=2) restoring ice
                                ↪   salinity, flushing (g/kg)
  rn_time_fl     =   8.64e+5    !   (nn_icesal=2) restoring time
                                ↪   scale, flushing (s)
  rn_simax       =   20.        !   maximum tolerated ice salinity
                                ↪   (g/kg)
  rn_simin       =   0.1        !   minimum tolerated ice salinity
                                ↪   (g/kg)

```

**Listing 9:** SI3 namelist, section ice salinity

The salinity of new ice is simply formulated as proportional to sea surface salinity:  $S^b = \nu S^w$ .  $\nu$  is a fractionation coefficient which depends on the basal ice growth rate (Cox and Weeks, 1988). The latter is outdated and should be replaced in forthcoming versions. The salinity of snow ice is a weighted mean of snow and seawater contributions.

There are two other sources of salt that are not included in the equation above associated with new ice formation in open water and porous ridging. The salinity of new ice formed in open water  $S_0$  is given by the S-h empirical relationship of Kovacs (1996).

For vertical thermodynamic computations, we assume that salinity has a vertical distribution  $S_k^i$ . Observations from ice cores suggest that the shape of the salinity profile in sea ice depends on bulk salinity. This is because the strongest changes in profile shape are due to flushing, which affects both the mean salinity and profile shape. Numerical experiments have shown that a linear profile well approximates the sea ice salinity profile. Therefore, we parameterize the shape of the salinity profile as follows. At high mean salinity, i.e., if  $\bar{S}^i > S_2 = 4.5$ , the profile is isosaline:  $S_k^i = S_\infty(z) = \bar{S}^i$ . At low mean salinity, i.e., if  $\bar{S}^i < S_1 = 3.5$ , the profile is linear:  $S_k^i = S_0(z)$ . This profile is determined by applying two constraints. First, its mean salinity should be equal to  $\bar{S}^i$  (given by 6.17), and second the salinity should be zero at the surface.

The global sea ice state variable associated to the ice salinity is the sea ice salt content, which is bulk salinity times volume of ice per unit area in each cate-

gory. As all extensive state variables  $M^s$  undergoes ridging and rafting, horizontal transport and transport in thickness space.

## 6.8 Single-category use

The number of ice categories directly relates to the CPU wall-clock time per year of simulation. `jp1= 5` ice categories is the default. Advanced users may use more, following recommendations by [Massonnet et al. \(2019\)](#), who tested up to 33. Reducing the number of categories below 5 deteriorates physics.

For those users who have no strong interest in properly resolving the sea ice thickness distribution and want to reduce the computer footprint of their sea ice calculations, there are parameterizations in the code that emulate the effects of a thickness distribution (which intensifies growth and melt), when using a single ice category. We speak of a *virtual* thickness distribution formulation

These parameterizations are activated with the namelist flag `ln_virtual_itd`. They were originally included in the LIM2 code from ideas developed in [Mellor and Kantha \(1989\)](#); [Fichefet and Morales Maqueda \(1997\)](#).

The first parameterization intensifies basal ice growth. Conduction of heat scales like the inverse ice thickness. Therefore, thin ice covered by thin snow grows much faster than thick ice with deep snow. Hence, models resolving the ITD grow more ice. The first parameterization aims at emulating this effect by intensifying ice growth. This is done by increasing the thermal conductivity of snow and ice, which is done in `ice_thd_zdf_b199` and `blk_ice_qcn`. Technically speaking, the conduction of heat scales like  $1/h_e$ , where  $h_e$  is a measure of combined snow and ice thickness. When `ln_virtual_itd` is true, the effective thermal conductivity of snow and ice is used  $k^{eff} = G.k$ , where  $G$  accounts for the unresolved thin ice:

$$G = \frac{1}{2} \left[ 1 + \ln \left( \frac{2h_e}{\epsilon} \right) \right]. \quad (6.18)$$

where  $\epsilon \approx 0.1$ , was regressed against a multi-category run.

The second parameterization intensifies melting. In multi-category models, thin ice disappears early on during the melt period, effectively reducing the ice concentration. This is an important process, since this opening of the pack triggers the ice-albedo feedback: shortwave radiation efficiently penetrates in the upper ocean, fostering basal sea ice melting. Single-category configurations cannot represent these physics. Simple scaling arguments show that the reduction in ice concentration scales like  $1/(2.h_i)$  ([Fichefet and Morales Maqueda, 1997](#)). To emulate the melting of thin ice, when `ln_virtual_itd` is activated, the ice concentration is reduced by  $A\Delta h/2$ , in `ice_thd_mono`.

## 6.9 Ice age

For diagnostic purposes, the ice age  $o_m^i$  of each thickness category is computed. Utilisation of age in marine modelling has shown that the values and interpretation of model age are strongly dependent on the age definition (see, e.g., [Deleersnijder et al., 2001](#)). We assume that the age is associated with the areal sea ice age content  $O_l = o_l^i g_l^i$ , which verifies:

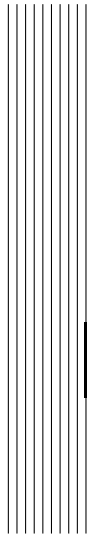
$$\frac{\partial O_l}{\partial t} = -\nabla \cdot (O_l \mathbf{u}) + \Theta_l^O + \Psi_l^O. \quad (6.19)$$

For coherence, first, the mechanical redistribution function associated to ice age  $\Psi^O$  is constructed based on  $\Psi^g$  (see earlier). Second, in contrast to [Harder and Lemke \(1994\)](#), vertical growth and melt do not affect the ice age (i.e., vertically accreted new ice is assumed to have the age of existing ice). Nevertheless, new ice formed in open water has an age equal to zero. Therefore, our value reflects an areal residence time, larger than the actual ice age, and the thermodynamic ageing term reads:

$$\Theta_l^O = g_l^i - \frac{\partial(f_l O_l)}{\partial h}, \quad (6.20)$$

where  $f_l$  is the sea ice growth/melt rate in the  $l^{\text{th}}$  category. The first term on the right-hand side represents ice ageing. The second term accounts for the formation of new ice in open water and for the transport in thickness space of the age content due to ice growth and melt. write





# 7

## Radiative transfer

### Contents

---

<b>7.1 Solar radiation partitioning in the snow-ice system . . . . .</b>	<b>65</b>
7.1.1 Surface albedo . . . . .	66
7.1.2 Transmission below the snow/ice surface . . . . .	69
7.1.3 Attenuation and transmission below the ice/ocean interface . . . . .	69
<b>7.2 Solar radiation: framing sea ice at the ocean-atmosphere boundary . . . . .</b>	<b>69</b>
7.2.1 Forced mode . . . . .	70
7.2.2 Coupled mode . . . . .	70

---

```

!-----
&namdyn_rdgfrft ! Ice ridging/rafting
!-----
      ! -- ice_rdgfrft_strength -- !
ln_str_H79      = .true.           ! ice strength param.: Hibler_79
  ↪ => P = pstar*<h>*exp(-c_rhg*A)
  rn_pstar      = 2.0e+04          ! ice strength thickness
  ↪ parameter [N/m2]
  rn_crhg       = 20.0             ! ice strength conc. parameter
  ↪ (-)
ln_str_R75      = .false.          ! ice strength param.: Rothrock_75
  ↪ => P = fn of potential energy
  rn_pe_rdg     = 17.0             ! coef accouting for frictional
  ↪ dissipation
ln_str_CST      = .false.          ! ice strength param.: Constant
  rn_str        = 0.0              ! ice strength value
ln_str_smooth   = .true.           ! spatial smoothing of the ice
  ↪ strength
      ! -- ice_rdgfrft -- !
ln_distf_lin    = .true.           ! redistribution function of ridged
  ↪ ice: linear (Hibler 1980)
ln_distf_exp    = .false.          ! redistribution function of ridged
  ↪ ice: exponential => not coded yet
  rn_murdg      = 3.0              ! e-folding scale of ridged ice
  ↪ (m**.5)
rn_csrdg        = 0.5              ! fraction of shearing energy
  ↪ contributing to ridging
      ! -- ice_rdgfrft_prep -- !
ln_partf_lin    = .false.          ! Linear ridging participation
  ↪ function (Thorndike et al, 1975)
  rn_gstar      = 0.15             ! fractional area of thin ice
  ↪ being ridged
ln_partf_exp    = .true.           ! Exponential ridging participation
  ↪ function (Lipscomb, 2007)
  rn_astar      = 0.03             ! exponential measure of ridging
  ↪ ice fraction [set to 0.05 if hstar=100]
ln_ridging      = .true.           ! ridging activated (T) or not (F)
  rn_hstar      = 25.0             ! determines the maximum
  ↪ thickness of ridged ice [m] (Hibler, 1980)
  rn_porordg    = 0.3              ! porosity of newly ridged ice
  ↪ (Lepparanta et al., 1995)
  rn_fsnwrldg   = 0.5              ! snow volume fraction that
  ↪ survives in ridging
  rn_fpndrdg    = 1.0              ! pond fraction that survives in
  ↪ ridging (small a priori)
ln_rafting      = .true.           ! rafting activated (T) or not (F)
  rn_hraft      = 0.75             ! threshold thickness for
  ↪ rafting [m]
  rn_craft      = 5.0              ! squeezing coefficient used in
  ↪ the rafting function
  rn_fsnwrft    = 0.5              ! snow volume fraction that
  ↪ survives in rafting
  rn_fpndrft    = 1.0              ! pond fraction that survives in
  ↪ rafting (0.5 a priori)

```

Listing 10: SI3 namelist, section ridging and rafting

Radiative transfer in SI<sup>3</sup> currently reduces to the parameterization of solar radiation partitioning through the snow/ice/open water system, treated using a single wavelength band. This will likely be improved in future versions of the code. In this chapter, we first explain how solar radiation is partitioned in the snow-ice system, then describe how, solar radiation-wise, the snow-ice system is framed in the context of the atmosphere-ice-ocean boundary.

## 7.1 Solar radiation partitioning in the snow-ice system

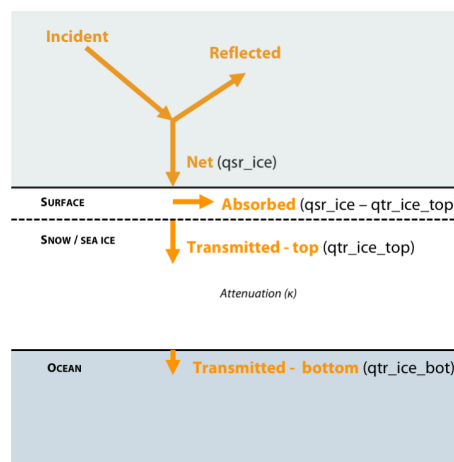


**Figure 7.1:** Partitioning of solar radiation in the snow-ice system, as represented in SI<sup>3</sup>.

Solar radiation in the snow-ice system is represented following the principles of [Maykut and Untersteiner \(1971\)](#), see Fig.7.4, using a unique band of solar radiation. Incident solar radiation ( $\text{W}/\text{m}^2$ , counted per unit ice area - not per grid cell area) is specified in the SBC routines and is a priori category dependent, because multiple atmosphere-surface reflexions are frequent in polar regions imply that incident radiation depends on the surface albedo and therefore surface state.

Net solar radiation  $\text{qsr\_ice}(i,j,l)$  is obtained by subtracting the reflected part of the incident radiation using the surface albedo  $\alpha(i,j,l)$ , parameterized as a function of environmental conditions.

The subsequent attenuation of solar radiation through the snow-ice system is represented assuming the presence of a highly diffusive surface scattering layer, absorbing a fraction  $i_o$  of net solar radiation, which is transformed into sensible heat, contributing to the surface energy balance.

The remainder of solar radiation,  $\text{qtr\_ice\_top}(i,j,l)$ , is transmitted below the surface and attenuates following Beer-Lambert law. The part of solar radiation that is absorbed on its path to the base of the ice is given as sensible heat to the snow/ice

system, via a source term in the heat diffusion equation. The rest of solar radiation that reaches the ice base,  $q_{tr\_ice\_bot}(i,j,l)$ , is transmitted to the ocean.

In the rest of this section, we describe how the albedo, the surface transmission parameter  $i_o$  and the attenuation of solar radiation are parameterized.

### 7.1.1 Surface albedo

The surface albedo determines the amount of solar radiation that is reflected by the ice surface, hence also net solar radiation. The philosophy of the parameterization of surface albedo is the following: each ice category has its own albedo value  $\alpha(i, j, l)$ , determined as a function of cloud fraction, ice thickness, snow depth, melt pond fraction and depth, using observation-based empirical fits.

The original [Shine and Henderson-Sellers \(1985\)](#) parameterization had a few inconsistencies and flaws that the revisited parameterization described hereafter fixes. In particular, the dependencies of albedos on ice thickness, snow depth and cloud fraction have been revised in the light of recent observational constraints ([Brandt et al., 2005](#); [Grenfell and Perovich, 2004](#)). In addition, the asymptotic properties of albedo are better specified and now fully consistent with oceanic values. Finally, the effect of melt ponds has been included ([Lecomte et al., 2015](#)).

The user has control on 5 reference namelist values, which describe the asymptotic values of albedo of snow and ice for dry and wet conditions, as well as the deep ponded-ice albedo. Observational surveys, in particular during SHEBA in the Arctic ([Perovich et al., 2002](#)) and further additional experiments ([Grenfell and Perovich, 2004](#)), as well as by [Brandt et al. \(2005\)](#) in the Antarctic, have provided relatively strong constraints on the surface albedo. In this context, the albedo can hardly be used as the main model tuning parameter, at least outside of these observation-based bounds (see `namalb` for reference values).

```

!-----
&namalb          !   albedo parameters
!-----
!
!   ↪   range (cloud-sky)
rn_alb_sdry      = 0.85      ! dry snow albedo           : 0.85
!   ↪   -- 0.87
rn_alb_smlt      = 0.75      ! melting snow albedo      : 0.72
!   ↪   -- 0.82
rn_alb_idry      = 0.60      ! dry ice albedo           : 0.54
!   ↪   -- 0.65
rn_alb_imlt      = 0.50      ! bare puddled ice albedo  : 0.49
!   ↪   -- 0.58
rn_alb_dpnd      = 0.27      ! ponded ice albedo       : 0.10
!   ↪   -- 0.30
rn_alb_hpiv      = 1.00      ! pivotal ice thickness in m (above
!   ↪   which albedo is constant)

```

Because the albedo is not an intrinsic optical property, it depends on the type of light (diffuse or direct), which is practically handled by weighting the clear (cs) and overcast (os) skies values by cloud fraction  $c(i, j)$  ([Fichefet and Morales Maqueda,](#)

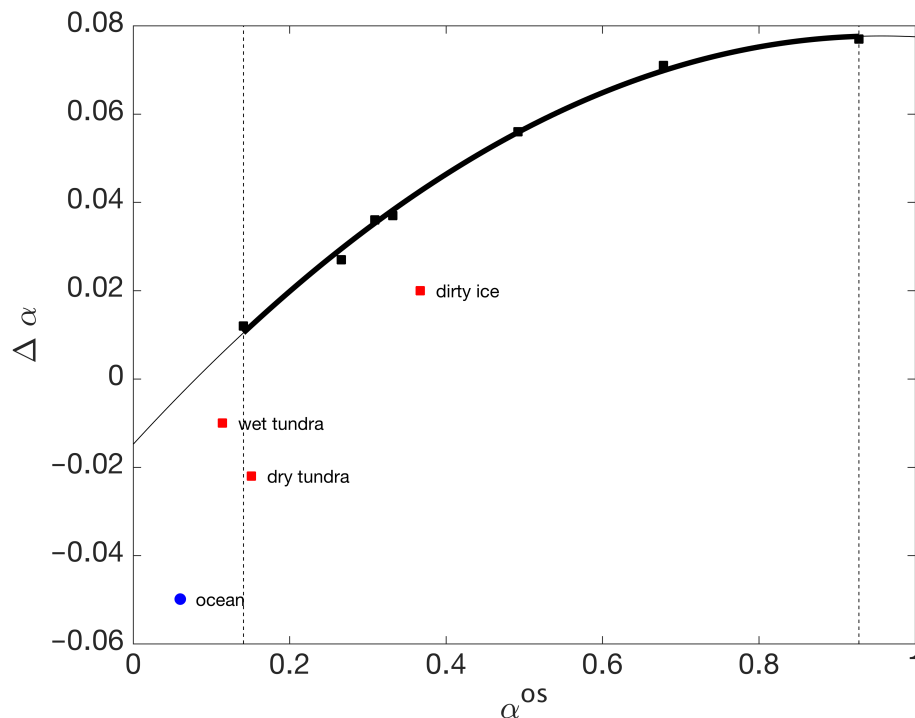


**Figure 7.2:** Albedo correction  $\Delta\alpha$  as a function of overcast sky (diffuse light) albedo  $\alpha_{os}$ , from field observations (Grenfell and Perovich, 2004, their Table 3) (squares) and 2nd-order fit (Eq. 7.3). Red squares represent the irrelevant data points excluded from the fit. For indication, the amplitude of the correction used in the ocean component is also depicted (blue circle).

1997):

$$\alpha(i, j, l) = [1 - c(i, j)] \cdot \alpha_{cs}(i, j, l) + c(i, j) \cdot \alpha_{os}(i, j, l). \quad (7.1)$$

For concision, we drop the spatial and category indices hereafter. Grenfell and Perovich (2004) observations at Point Barrow, on the Alaskan Coast, suggest that clear and overcast sky albedos are directly related through

$$\alpha_{cs} = \alpha_{os} - \Delta\alpha(\alpha_{os}). \quad (7.2)$$

The relation between  $\Delta\alpha$  and  $\alpha_{os}$  can well be handled using a 2<sup>nd</sup>-order polynomial fit (Fig. 7.2):

$$\Delta\alpha = (-0.1010 \cdot \alpha_{os}^2 + 0.1933 \cdot \alpha_{os} - 0.0148). \quad (7.3)$$

Overcast sky surface albedo is used as a reference, from which the clear-sky value is derived.

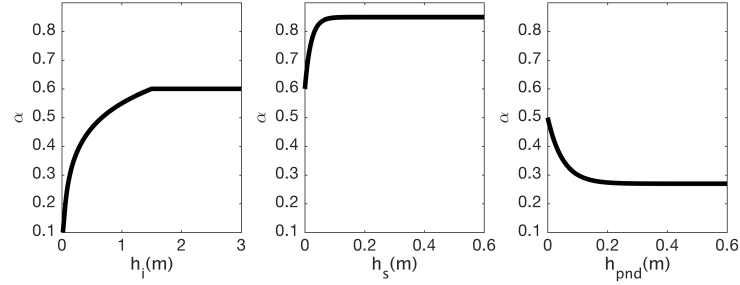


**Figure 7.3:** Example albedo dependencies on ice thickness, snow depth and pond depth, as parameterized in SI<sup>3</sup>.

The second important parameter that controls surface albedo is surface type. In each category, we assume that three types of surfaces can coexist (bare, snow-covered and ponded ice), with respective fractions  $f_{ice}$ ,  $f_{snow}$  and  $f_{pnd}$  summing to 1. Then the overcast albedo is expressed as

$$\alpha_{os}(i, j, l) = f_{ice} \cdot \alpha_{ice} + f_{snow} \cdot \alpha_{snow} + f_{pnd} \cdot \alpha_{pnd} \quad (7.4)$$

with a specific albedo value for each surface type.

The surface fractions  $f_{ice}$ ,  $f_{snow}$  and  $f_{pnd}$  are currently crudely parameterized: if snow is present ( $h_s > 0$ ), then  $f_{snow} = 1$  and  $f_{ice} = f_{pnd} = 0$ . In the absence of snow,  $f_{pnd}$  is either specified or calculated (depending on melt pond options in nam\_pnd), and  $f_{ice} = 1 - f_{pnd}$ . Admittedly, more refined parameterizations of  $f_{snow}$  could improve the realism of the model. Note finally that the dependence of surface albedo on the presence of melt ponds can be included or not (namelist parameter `ln_pnd_alb`). If the latter is set to false,  $f_{pnd}$  is always assumed zero in the albedo computations.

Works by [Brandt et al. \(2005\)](#) and references therein, indicate that the dependence of the albedo of bare ice on ice thickness depends is linear/logarithmic/constant from thin to thick ice. Hence, the following expressions capture the essence of their works:

$$\alpha_{ice} = \begin{cases} \alpha_{ice}^{\infty} & \text{if } h_i > 1.5, \\ \alpha_{ice}^{\infty} + (0.18 - \alpha_{ice}^{\infty}) \cdot \frac{\ln(1.5) - \ln(h_i)}{\ln(1.5) - \ln(0.05)} & \text{if } 0.05 < h_i, \leq 1.5 \\ \alpha_{ice}^{\infty} + (0.18 - \alpha_{ice}^{\infty}) h_i / 0.05 & \text{if } h_i < 0.05. \end{cases} \quad (7.5)$$

The thick-ice constant albedo value depends on whether the surface is dry or melting:

$$\alpha_{ice}^{\infty} = \begin{cases} \alpha_{i,dry} & \text{if } T_{su} < T_{fr} \\ \alpha_{i,mlt} & \text{if } T_{su} = T_{fr}, \end{cases} \quad (7.6)$$

values that are to be specified from the namelist.

Grenfell and Perovich (2004) suggest that the dependence of surface albedo on snow depth is exponential,

$$\alpha_{snow} = \alpha_{snow}^{\infty} - (\alpha_{snow}^{\infty} - \alpha_{ice}) * \exp(-h_s/h_s^{ref}), \quad (7.7)$$

where  $h_s^{ref} = 0.02$  (0.03) m for dry (wet) snow. As for bare ice, the deep-snow asymptotic albedo also depends on whether the surface is dry or melting:

$$\alpha_{snow}^{\infty} = \begin{cases} \alpha_{s,dry} & \text{if } T_{su} < T_{fr} \\ \alpha_{s,mlt} & \text{if } T_{su} = T_{fr}, \end{cases} \quad (7.8)$$

values that are to be specified from the namelist.

Based on ideas developed from melt ponds on continental ice (Zuo and Oerlemans, 1996), the albedo of ponded ice was proposed to follow (Lecomte et al., 2011):

$$\alpha_{pnd} = \alpha_{dpnd} - (\alpha_{dpnd} - \alpha_{ice}) \cdot \exp(-h_{pnd}/0.05) \quad (7.9)$$

$\alpha_{dpnd}$  is a namelist parameter. Ebert and Curry (1993) also use such dependency for their multi-spectral albedo.

The dependencies of surface albedo on ice thickness, snow depth and pond depth are illustrated in Fig. 7.3.

### 7.1.2 Transmission below the snow/ice surface

The transmitted solar radiation below the surface is represented following Fichet and Morales Maqueda (1997) and Maykut and Untersteiner (1971):

$$qtr\_ice\_top(i, j, l) = i_o(i, j) qsr\_ice(i, j, l), \quad (7.10)$$

where  $i_o = 0$  in presence of snow, and depends on cloud fraction otherwise, based on works of Grenfell and Maykut (1977). This parameterization needs to be re-evaluated and likely updated.

### 7.1.3 Attenuation and transmission below the ice/ocean interface

Attenuation of solar radiation through the ice follows Beer-Lambert law. In practise, we assume that irradiance below layer  $k$  is given by

$$radtr\_i(i, j, k, l) = qtr\_ice\_top(i, j, l) \cdot \exp(-\kappa_i z), \quad (7.11)$$

where  $\kappa_i = 1 \text{ m}^{-1}$  is the exponential attenuation coefficient (namelist parameter `rn_kappa_i`). Hence, at the ice base, remains below the  $l^{th}$  category a transmitted flux:

$$qtr\_ice\_bot(i, j, l) = qtr\_ice\_top(i, j, l) \cdot \exp(-\kappa_i h_i). \quad (7.12)$$

## 7.2 Solar radiation: framing sea ice at the ocean-atmosphere boundary

How solar radiation transfer through sea ice is framed into the atmosphere-ice-ocean is nearly identical but not exactly the same in forced and coupled mode (see Fig. 7.4).

The basic principle of the computation is that the irradiant flux given to the ocean model (qsr) is computed as the average flux per grid cell area (qsr\_tot) minus what is given to the sea ice ( $\sum a(l)qsr\_ice(l)$ ), plus what is transmitted below sea ice  $\sum qtr\_ice\_bot(jl)$  (see at the base of Fig. 7.4). Such formulation ensures heat conservation by construction.

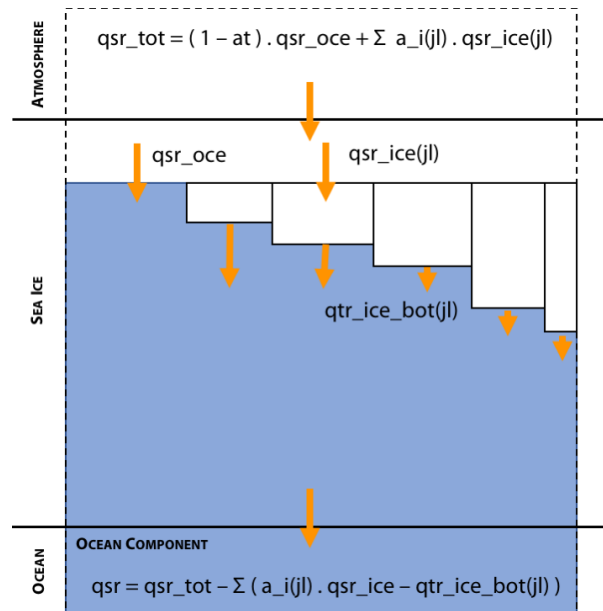


**Figure 7.4:** Framing solar radiation transfer through sea ice into the atmosphere-ice-ocean context.

### 7.2.1 Forced mode

In forced-atmosphere mode, it is the incoming solar irradiance fluxes above the ocean and sea ice (categories) that are specified (from files) or computed (from bulk formulae), and constitute the basis of solar radiation transfer computations. Then the net solar fluxes above open water (qsr\_oce) and ice categories (qsr\_ice) are obtained by multiplication by  $1 - \alpha$ . qsr\_tot is then diagnosed as a weighted sum of qsr\_oce and the qsr\_ice(jl)'s.

### 7.2.2 Coupled mode

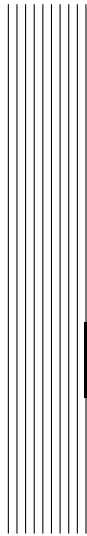
In coupled-atmosphere mode,  $qsr\_tot$  and  $qsr\_ice$  have to be provided by the atmospheric model, whereas  $qsr\_oce$  is diagnosed from  $qsr\_ice$  and  $qsr\_tot$ .

Some atmospheric models enable *tiling* and can provide solar fluxes over individual ice categories. For such atmospheric models, net solar radiation fluxes are directly useable by SI<sup>3</sup> ( $nn\_flxdist = -1$ ). Other models cannot do tiling, being only able to provide a net solar flux above all ice categories, seen as a single surface type. For such models a first option is to give the net solar flux above sea ice identically to all sea ice categories ( $nn\_flxdist = 0$ ). Yet a better option is to redistribute the mean solar flux above sea ice  $\langle qsr\_ice \rangle$  above categories ( $nn\_flxdist = 2$ ) using the following scaling, conserving heat by construction:

$$qsr\_ice(jl) = \langle qsr\_ice \rangle \frac{1 - \alpha(jl)}{1 - \langle \alpha \rangle} \quad (7.13)$$

where  $\langle \alpha \rangle$  is the albedo averaged over the ice categories. Note that for testing, the flux redistributor can be emulated in forced mode ( $nn\_flxdist = 1$ ).





## 8 Output and diagnostics

### Contents

---

<b>8.1 SIMIP diagnostics</b> . . . . .	<b>74</b>
8.1.1 Missing SIMIP fields . . . . .	74
8.1.2 Links . . . . .	75
<b>8.2 Conservation checks</b> . . . . .	<b>75</b>

---

## 8.1 SIMIP diagnostics

The SIMIP protocol (Notz et al., 2016) was designed for CMIP6, to standardize sea ice model outputs in climate simulations. We tried to follow the data request as closely as possible. Outputs are in most cases directly managed with XIOS2 in `limwri.F90`, but not always. In the code, output fields keep their native LIM reference name.

A corresponding entry exists in `field_def_nemo-lim.xml`, where fields are given their SIMIP specifications (standard name, long name, units). At the end of the file the fields are gathered in the field groups `SIday_fields`, `SImon_fields` and `SImon_scalar` for separation of the daily (SIday) and monthly (SImon) requests.

In `file_def_nemo-lim.xml`, the daily, monthly and scalar output files are created.

In the reference xml files, the largest possible SIMIP-based diagnostics with LIM are distributed among the field groups. If some fields are to be discarded, the best way to do so is to remove them from the field groups in `field_def_nemo-lim.xml`.

### 8.1.1 Missing SIMIP fields

About 90% of the SIMIP fields can be output. Below is the list of the missing fields and why they are missing.

#### 1. Fields that are not part of the sea ice representation in LIM3.6

- `sisnconc` (snow area fraction), `siitdsnconc` (snow area fractions in thickness categories);
- `simpconc` (meltpond area fraction), `simpmass` (melt pond mass per area), `simprefrozen` (thickness of refrozen ice on ponds);
- `sirdgconc` (ridged ice area fraction), `sirdgmass` (ridged ice thickness);
- `sidmasslat` (lateral sea ice melt rate);
- `sndmasswindrif` (snow mass change through wind drift of snow);

#### 2. Fields which value is trivial

- `sipr` (rainfall over sea ice): all rain falls in open water;
- `sidragtop` (atmospheric drag over sea ice): namelist parameter;
- `sidragbot` (oceanic drag over sea ice): namelist parameter

### 3. Fields that belong to the atmospheric component

- siflswdtop, siflswutop, siflswdbot, sifllwdtop, sifllwutop, siflsenstop, sifflat-stop (surface energy budget components)

Ice thickness and snow depth were masked below 5% ice concentration, because below this value, they become meaninglessly large in LIM. This is notably because of the Prather advection scheme. We hope to fix these issues for our next release. For similar reasons, the ice age is masked below 15% concentration.

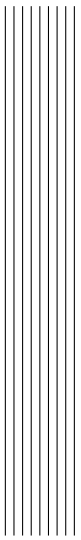
Fluxes through straits and passages were not directly implemented. Instead, ice mass, snow mass, and ice area transports were implemented as 2D arrays, for x- and y- directions. A python script is available to derive the fluxes through straits and passages from full 2D arrays for ORCA2 and eORCA1 grids.

#### 8.1.2 Links

- [Paper of Notz et al](#);
- [SIMIP CMIP6 data request page](#);
- [SIMIP description on CliC website](#).

## 8.2 Conservation checks





## 9

# Guidelines for documenting the code

Each chapter of the documentation could follow the following guidelines.

Doc is not meant to duplicate the code, rather it is meant to help users know about physics and numerics, walk through the code, find key references and understand namelist parameters.

Doc responds to basic questions user may have on why coding choices were made, and should be shorter than the code itself.

## Introduction

A few sentences along these lines:

1. Define the chain of processes the chapter refers to.
2. Key calculation in the model.
3. Outline model representation
4. Key inputs (possibly different for each variant)
5. Impact on model variables

### 9.1 Overarching aspects and practical features

Describe in more detail how the physics are decomposed in the model representation. Locate the main subroutine call and other important steps. Describe key code infrastructure choices. Mention specific aspects of interest. All global namelist parameters must have been described here.

## 9.2 Calculation step 1

1 figure if needed.

Overview of the method (input, output, method).

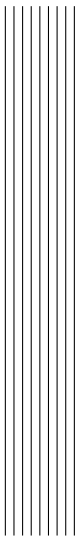
Input fields and why they are needed.

Some description of the calculation. Make sure all namelist parameters are described.

Output fields and what controls them.

[ All local namelist parameters must have been described here].

## 9.3 Calculation step 2



## Bibliography

- Assur, A., 1958: Composition of sea ice and its tensile strength. *A. Nat. Acad. Sci./Nat. Res. Council, Arctic Sea Ice*, **598**, 106–138.
- Babko, O., D. A. Rothrock, and G. A. Maykut, 2002: Role of rafting in the mechanical redistribution of sea ice thickness. *Journal of Geophysical Research*, **107**, 3113, doi:10.1029/1999JC000190, doi:doi:10.1029/1999JC000190.
- Biggs, N. R. T., M. A. M. Maqueda, and A. J. Willmott, 2000: Polynya flux model solutions incorporating a parameterization for the collection thickness of consolidated new ice. *Journal of Fluid Mechanics*, **408**, 179–204.
- Bitz, C. M., M. M. Holland, A. J. Weaver, and M. Eby, 2001: Simulating the ice-thickness distribution in a coupled climate model. *Journal of Geophysical Research: Oceans*, **106 (C2)**, 2441–2463, doi:10.1029/1999JC000113.
- Bitz, C. M. and W. H. Lipscomb, 1999: An energy-conserving thermodynamic model of sea ice. *Journal of Geophysical Research*, **104**, 15,669–15,677.
- Blockley, E., M. Vancoppenolle, E. Hunke, C. Bitz, D. Feltham, J.-F. Lemieux, M. Losch, E. Maisonnave, D. Notz, P. Rampal, S. Tietsche, B. Tremblay, A. Turner, F. Massonnet, E. Ólason, A. Roberts, Y. Aksenov, T. Fichefet, G. Garric, D. Iovino, G. Madec, C. Rousset, D. Salas y Melia, and D. Schroeder, 2020: The Future of Sea Ice Modeling: Where Do We Go from Here? *Bulletin of the American Meteorological Society*, **101 (8)**, E1304–E1311, doi:10.1175/BAMS-D-20-0073.1, URL <http://journals.ametsoc.org/bams/article/101/8/E1304/346483/The-Future-of-Sea-Ice-Modeling-Where-Do-We-Go-from>, publisher: American Meteorological Society.
- Bouillon, S., T. Fichefet, V. Legat, and G. Madec, 2013: The elastic-viscous-plastic method revisited. *Ocean Modelling*, **71**, 2–12.
- Brandt, R. E., S. G. Warren, A. P. Worby, and T. C. Grenfell, 2005: Surface albedo of the Antarctic sea ice zone. *Journal of Climate*, **18**, 3606–3622.
- Connolley, W. M., J. Gregory, E. Hunke, and A. McLaren, 2004: On the consistent scaling of terms in the sea-ice dynamics equation. *Journal of Physical Oceanography*, **34(7)**, 1776–1780.

- Coon, M. D., G. A. Maykut, R. S. Pritchard, D. A. Rothrock, and A. S. Thorndike, 1974: Modeling the pack ice as an elastic-plastic material. *AIDJEX Bulletin*, **24**, 1–105.
- Cox, G. F. N. and W. F. Weeks, 1988: Numerical simulations of the profile properties of undeformed first-year sea ice during growth season. *Journal of Geophysical Research*, **93**, 12,449–12,460.
- Deleersnijder, E., J.-M. Campin, and E. J. M. Delhez, 2001: The concept of age in marine modelling: I. Theory and preliminary model results. *Journal of Marine Systems*, **28**, 229–267.
- Ebert, E. E. and J. A. Curry, 1993: An intermediate one-dimensional thermodynamic sea ice model for investigating ice-atmosphere interactions. *Journal of Geophysical Research*, **98**, 10,085–10,109.
- Feistel, R. and W. Wagner, 2006: A New Equation of State for H<sub>2</sub>O Ice Ih. *J. Phys. Chem. Ref. Data*, **35**, 1021–1047.
- Feltham, D. L., 2008: Sea Ice Rheology. *Annual Review of Fluid Mechanics*, **40** (1), 91–112, doi:10.1146/annurev.fluid.40.111406.102151, URL <https://doi.org/10.1146/annurev.fluid.40.111406.102151>.
- Fichefet, T. and P. Gaspar, 1988: A Model Study of Upper Ocean-Sea Ice Interactions. *Journal of Physical Oceanography*, **18** (2), 181–195, doi:10.1175/1520-0485(1988)018<0181:AMSOUO>2.0.CO;2, URL [https://journals.ametsoc.org/view/journals/phoc/18/2/1520-0485\\_1988\\_018\\_0181\\_amsouo\\_2\\_0\\_co\\_2.xml](https://journals.ametsoc.org/view/journals/phoc/18/2/1520-0485_1988_018_0181_amsouo_2_0_co_2.xml), publisher: American Meteorological Society Section: Journal of Physical Oceanography.
- Fichefet, T. and M. A. Morales Maqueda, 1997: Sensitivity of a global sea ice model to the treatment of ice thermodynamics and dynamics. *Journal of Geophysical Research*, **102**, 12,609–12,646.
- Flato, G. M. and W. D. Hibler, 1995: Ridging and strength in modeling the thickness distribution of Arctic sea ice. *Journal of Geophysical Research*, **100**, 18 611–18 626.
- Flocco, D. and D. L. Feltham, 2007: A continuum model of melt pond evolution on Arctic sea ice. *Journal of Geophysical Research*, **112**, C08 016, doi:10.1029/2006JC003 836, doi:doi:10.1029/2006JC003836.
- Grenfell, T. C. and G. A. Maykut, 1977: The optical properties of ice and snow in the Arctic Basin. *Journal of Glaciology*, **18**, 445–463.
- Grenfell, T. C. and D. K. Perovich, 2004: Seasonal and spatial evolution of albedo in a snow-ice-land-ocean environment. *Journal of Geophysical Research: Oceans*, **109** (C1), doi:10.1029/2003JC001866, URL <https://onlinelibrary.wiley.com/doi/abs/10.1029/2003JC001866>, \_eprint: <https://agupubs.onlinelibrary.wiley.com/doi/pdf/10.1029/2003JC001866>.
- Haapala, J., 2000: On the modelling of ice-thickness redistribution. *Journal of Glaciology*, **46** (154), 427–437.
- Harder, M. and P. Lemke, 1994: Modelling the Extent of Sea Ice Ridging in the Weddell Sea. *The Polar Oceans and their role in shaping the global environment*, Johannessen, O. M., R. D. Muench, and J. E. Overland, Eds., American Geophysical union, Geophysical Monograph, Vol. The Nansen Centennial Volume 85, 187–197.
- Hibler, W. D., 1979: A dynamic thermodynamic sea ice model. *Journal of Physical Oceanography*, **9**, 815–846.
- , 1980: Modeling a variable thickness sea ice cover. *Monthly Weather Review*, **108**, 1943–1973.
- Høyland, 2002: Consolidation of first-year sea ice ridges. *Journal of Geophysical Research*, **107**, 3062, doi:10.1029/2000JC000 526, doi:doi:10.1029/2000JC000526.
- Hunke, E. and J. K. Dukowicz, 2002: The elastic-viscous-plastic sea ice dynamics model in general orthogonal curvilinear coordinates on a sphere-incorporation of metric terms. *Monthly Weather Review*, **130**, 1848–1865.
- IOC, SCOR and IAPSO, 2010: The international thermodynamic equation of seawater - 2010: Cal-

- ulation and use of thermodynamic properties. Intergovernmental Oceanographic Commission, Manuals and Guides 56, UNESCO.
- Josberger, E. G. and S. Martin, 1981: A laboratory and theoretical study of the boundary layer adjacent to a vertical melting ice wall in salt water. *Journal of Fluid Mechanics*, **111**, 439–473, doi:10.1017/S0022112081002450, URL <https://www.cambridge.org/core/journals/journal-of-fluid-mechanics/article/abs/laboratory-and-theoretical-study-of-the-boundary-layer-adjacent-to-a-vertical-melting-ice-A48BDAF475F57BB397331499FCDED917>, publisher: Cambridge University Press.
- Jutras, M., M. Vancoppenolle, A. Lourenço, F. Vivier, G. Carnat, G. Madec, C. Rousset, and J.-L. Tison, 2016: Thermodynamics of slush and snow ice formation on sea ice. *Deep-Sea Research II*, **131**, 75–83, doi:10.1016/j.dsr2.2016.03.008.
- Kovacs, A., 1996: Sea ice, Part I. Bulk salinity versus ice floe thickness. Tech. Rep. 96-7, Cold Regions Research and Engineering Laboratory, Hanover, New Hampshire.
- Lebrun, M., 2019: De l'interaction entre banquise, lumière et phytoplancton arctique.
- Lecomte, O., T. Fichefet, D. Flocco, D. Schroeder, and M. Vancoppenolle, 2015: Interactions between wind-blown snow redistribution and melt ponds in a coupled ocean-sea ice model. *Ocean Modelling*, **87**, 67–80, doi:10.1016/j.ocemod.2014.12.003.
- Lecomte, O., T. Fichefet, M. Vancoppenolle, and M. Nicolaus, 2011: A new snow thermodynamic scheme for large-scale sea-ice models. *Annals of Glaciology*, **52**, 337–346.
- Lemieux, J.-F. and F. Dupont, 2020: On the calculation of normalized viscous–plastic sea ice stresses. *Geoscientific Model Development*, **13** (3), 1763–1769, doi:https://doi.org/10.5194/gmd-13-1763-2020, URL <https://gmd.copernicus.org/articles/13/1763/2020/>, publisher: Copernicus GmbH.
- Lemieux, J.-F. and B. Tremblay, 2009: Numerical convergence of viscous-plastic sea ice models. *Journal of Geophysical Research: Oceans*, **114** (C5), doi:10.1029/2008JC005017, URL <https://agupubs.onlinelibrary.wiley.com/doi/abs/10.1029/2008JC005017>, eprint: <https://agupubs.onlinelibrary.wiley.com/doi/pdf/10.1029/2008JC005017>.
- Leppäranta, M., 2005: *The Drift of Sea ice*. Springer.
- Leppäranta, M., M. Lensu, and P. K. B. Witch, 1995: The life story of a first-year sea ice ridge. *Cold Regions Science and Technology*, **23**(3), 279–290.
- Lipscomb, W. H., 2001: Remapping the thickness distribution in sea ice models. *Journal of Geophysical Research*, **106**, 13 989–14 000.
- Lipscomb, W. H., E. Hunke, W. Maslowski, and J. Jackaci, 2007: Ridging, strength, and stability in high-resolution sea ice models. *Journal of Geophysical Research*, **112**, doi:10.1029/2005JC003355.
- Losch, M., D. Menemenlis, J.-M. Campin, P. Heimbach, and C. Hill, 2010: On the formulation of sea-ice models. Part 1: Effects of different solver implementations and parameterizations. *Ocean Modelling*, **33** (1), 129–144, doi:10.1016/j.ocemod.2009.12.008, URL <http://www.sciencedirect.com/science/article/pii/S1463500309002418>.
- Lüpkes, C., V. M. Gryanik, J. Hartmann, and E. L. Andreas, 2012: A parametrization, based on sea ice morphology, of the neutral atmospheric drag coefficients for weather prediction and climate models. *Journal of Geophysical Research: Atmospheres*, **117** (D13), doi:10.1029/2012JD017630, URL <https://onlinelibrary.wiley.com/doi/abs/10.1029/2012JD017630>, eprint: <https://onlinelibrary.wiley.com/doi/pdf/10.1029/2012JD017630>.
- Massonnet, F., A. Barthélemy, K. Worou, T. Fichefet, M. Vancoppenolle, C. Rousset, and E. Moreno-Chamarro, 2019: On the discretization of the ice thickness distribution in the NEMO3.6-LIM3 global ocean–sea ice model. *Geoscientific Model Development*, **12** (8), 3745–3758, doi:10.5194/gmd-12-3745-2019, URL <https://gmd.copernicus.org/articles/12/3745/2019/>, publisher: Copernicus GmbH.

- Maykut, G. A., 1986: The surface heat and mass balance. *The Geophysics of sea ice*, Untersteiner, N., Ed., Plenum Press, New York, NATO ASI Series. Series B, Physics., Vol. 146, 395–463.
- Maykut, G. A. and M. G. McPhee, 1995: Solar heating of the Arctic mixed layer. *Journal of Geophysical Research*, **100**, 24,691–24,703.
- Maykut, G. A. and D. K. Perovich, 1987: The role of shortwave radiation in the summer decay of a sea ice cover. *Journal of Geophysical Research: Oceans*, **92** (C7), 7032–7044, doi:10.1029/JC092iC07p07032, URL <http://onlinelibrary.wiley.com/doi/abs/10.1029/JC092iC07p07032>, \_eprint: <https://agupubs.onlinelibrary.wiley.com/doi/pdf/10.1029/JC092iC07p07032>.
- Maykut, G. A. and A. S. Thorndike, 1973: An approach to coupling the dynamics and thermodynamics of Arctic sea ice. *AIDJEX Bulletin*, **21**, 23–29.
- Maykut, G. A. and N. Untersteiner, 1971: Some results from a time-dependent thermodynamic model of sea ice. *Journal of Geophysical Research*, **76**, 1550–1575.
- McPhee, M. G., 1992: Turbulent heat flux in the upper ocean under sea ice. *Journal of Geophysical Research*, **97**(C4), 5365–5379.
- Mellor, G. L. and L. Kantha, 1989: An Ice-Ocean Coupled Model. *Journal of Geophysical Research*, **94**, 10,937–10,954.
- Notz, D., A. Jahn, M. Holland, E. Hunke, F. Massonnet, J. Stroeve, B. Tremblay, and M. Vancoppenolle, 2016: The CMIP6 Sea-Ice Model Intercomparison Project (SIMIP): understanding sea ice through climate-model simulations. *Geoscientific Model Development*, **9** (9), 3427–3446.
- Parmerter, R. R., 1975: A model of simple rafting in sea ice. *Journal of Geophysical Research*, **80**, 1948–1952.
- Perovich, D. K., T. C. Grenfell, B. Light, and P. V. Hobbs, 2002: Seasonal evolution of the albedo of multiyear Arctic sea ice. *Journal of Geophysical Research*, **107**, 8044, doi:10.1029/2000JC000438, doi:doi:10.1029/2000JC000438.
- Pounder, E. R., 1965: *The Physics of Ice*. Pergamon Press, Oxford, UK.
- Prather, M. J., 1986: Numerical advection by conservation of second-order moments. *Journal of Geophysical Research*, **91**, 6671–6681.
- Pringle, D. J., H. Eicken, H. J. Trodahl, and L. G. E. Backstrom, 2007: Thermal conductivity of landfast Antarctic and Arctic sea ice. *Journal of Geophysical Research*, **112**, doi:10.1029/2006JC003641, doi:10.1029/2006JC003641.
- Rothrock, D. and A. S. Thorndike, 1984: Measuring the sea ice floe size distribution. *Journal of Geophysical Research*, **89**, 6477–6486.
- Schmidt, G., C. M. Bitz, U. Mikolajewicz, and L.-B. Tremblay, 2004: Ice-ocean boundary conditions for coupled models. *Ocean Modelling*, **7**, 59–74, doi:doi:10.1016/S1463-5003(03)00030-1.
- Shine, K. P. and A. Henderson-Sellers, 1985: The sensitivity of a thermodynamic sea ice model to changes in surface albedo parameterization. *Journal of Geophysical Research*, **90**, 2243–2250.
- Thorndike, A. S., D. A. Rothrock, G. A. Maykut, and R. Colony, 1975: The thickness distribution of sea ice. *Journal of Geophysical Research*, **80**, 4501–4513.
- Tsamados, M., D. L. Feltham, and A. V. Wilchinsky, 2013: Impact of a new anisotropic rheology on simulations of Arctic sea ice. *Journal of Geophysical Research: Oceans*, **118** (1), 91–107, doi:10.1029/2012JC007990, URL <https://onlinelibrary.wiley.com/doi/abs/10.1029/2012JC007990>, \_eprint: <https://onlinelibrary.wiley.com/doi/pdf/10.1029/2012JC007990>.
- Tuhkuri, J. and M. Lensu, 2002: Laboratory tests on ridging and rafting of ice sheets. *Journal of Geophysical Research*, **107**, 3125, doi:10.1029/2001JC000848, doi:doi:10.1029/2001JC000848.
- Untersteiner, N., 1964: Calculations of temperature regime and heat budget of sea ice in the Central Arctic. *Journal of Geophysical Research*, **69**, 4755–4766.

- Vancoppenolle, M., T. Fichefet, and H. Goosse, 2009a: Simulating the mass balance and salinity of Arctic and Antarctic sea ice. 2. Sensitivity to salinity processes. *Ocean Modelling*, **27** (1–2), 54–69, doi:10.1016/j.ocemod.2008.11.003.
- Vancoppenolle, M., T. Fichefet, H. Goosse, S. Bouillon, G. Madec, and M. A. Morales Maqueda, 2009b: Simulating the mass balance and salinity of Arctic and Antarctic sea ice. 1. Model description and validation. *Ocean Modelling*, **27** (1–2), 33–53, doi:10.1016/j.ocemod.2008.10.005.
- Wang, Z., L. Youyu, D. G. Wright, and F. Dupont, 2010: Sea ice sensitivity to the parameterisation of open water area. *Journal of Operational Oceanography*, **3**, 1–9.
- West, A. E., A. J. McLaren, H. T. Hewitt, and M. J. Best, 2016: The location of the thermodynamic atmosphere–ice interface in fully coupled models – a case study using JULES and CICE. *Geoscientific Model Development*, **9** (3), 1125–1141, doi:10.5194/gmd-9-1125-2016, URL <https://gmd.copernicus.org/articles/9/1125/2016/>, publisher: Copernicus GmbH.
- Wilchinsky, A. V., D. L. Feltham, and P. A. Miller, 2006: A Multithickness Sea Ice Model Accounting for Sliding Friction. *Journal of Physical Oceanography*, **36**, 1719–1738.
- Worster, M. G., 1992: The Dynamics of Mushy Layers. *Interactive dynamics of convection and solidification*, Davis, S. H., H. E. Huppert, U. Müller, and M. G. Worster, Eds., Kluwer, 113–138.
- Zhang, J. and W. D. Hibler, 1997: On an efficient numerical method for modeling sea ice dynamics. *Journal of Geophysical Research*, **102**, 8691–8702.
- Zhang, J. and D. Rothrock, 2001: A thickness and enthalpy distribution sea ice model. *Journal of Physical Oceanography*, **31**, 2986–3001.
- Zuo, Z. and J. Oerlemans, 1996: Modelling albedo and specific balance of the Greenland ice sheet: calculations for the Søndre Strømfjord transect. *Journal of Glaciology*, **42** (141), 305–317, doi:10.3189/S0022143000004160, URL <https://www.cambridge.org/core/journals/journal-of-glaciology/article/modelling-albedo-and-specific-balance-of-the-greenland-ice-sheet-calculations-for-the-sondre-strømfjord-transect>, publisher: Cambridge University Press.



